PHYSICAL REVIEW VOLUME 149, NUMBER 1 9 SEPTEMBER 1966

Nuclear Quadrupole Resonance by Nuclear Induction: Theory and Experiment; with an Extension of the Theory to Absorption Methods

GEORGE W. SMITH
General Motors Research Laboratories, Warren, Michigan

(Received 23 February 1966; revised manuscript received 23 May 1966)

A theory is presented for nuclear quadrupole resonance (NQR) by means of nuclear induction and is extended to absorption methods. Based on the Bloch-type equations of Bloom, Robinson, and Volkoff, the theory is derived for the case $I=1$, $\eta=0$. For the induction method to work, a small magnetic field must remove the degeneracy of the $m=\pm1$ levels; in practice this is done by an audio-frequency modulation field. Phase-sensitive detection methods are then used to minimize noise. The theory predicts the effect of modulation field, static magnetic field, and rf field on the slow-passage induction signal. Theory and experiment agree that magnetic fields (modulating or static) broaden the line, but for low enough fields, the true NQR derivative line is observed. Sufficiently large static fields introduce complex structure into the line shape. The effect of rf is given by a modified form of the Bloembergen-Purcell-Pound saturation curves. Experiments on polycrystal hexamethylenetetramine yield good agreement with all aspects of the theory. The extension of the theory to single-coil (absorption) NQR methods predicts that sinusoidal magnetic modulation and phase-sensitive detection will produce zero signal in a single-coil experiment. In addition it yields the proper line shapes for Zeeman modulation and frequency modulation methods and predicts the effects of modulation amplitude and magnetic fields in both cases. A brief qualitative discussion of cases other than $I=1$, $\eta=0$ indicates that the induction method can be used for half-integral spins with any η, but that it is applicable to integral spins only when η is small. In other words the induction method can be used for any case to which the Zeeman-modulated absorption method is applicable.

I. INTRODUCTION

ALTHOUGH nuclear quadrupole resonance (NQR) experiments using a two-coil nuclear induction spectrometer were first performed ten years ago by Haering and Volkoff[1] and continued by Robinson,[2] it has been only recently that interest in this experimental method has become more widespread.[3–5] The availability of commercial instruments of this type promises to make the induction spectrometer a valuable supplement to the already commonly used single-coil absorption devices of both the frequency-modulated and Zeeman-modulated varieties.

In principle the induction method is unsuitable for NQR.[6–8] However, the presence of a magnetic field can permit the method to work.[6,9,10] A qualitative discussion of the method of NQR using the two-coil induction spectrometer is given in Ref. 4. Pulse-type induction experiments are discussed in Refs. 9 and 10.

As is well known,[6,8,10] the reason for the failure of the induction method in the absence of a magnetic field lies in the twofold degeneracy of the $m_I>0$ levels. In terms of the classical precession picture (for cylindrical symmetry, $\eta=0$), magnetizations aligned at angles θ and $\theta+\pi$ with respect to the field-gradient direction have precession frequencies equal in magnitude but opposite in sense.[11,12] As a consequence, voltages induced in a nuclear induction pickup coil by the two components exactly cancel. In this sense, then, the induction method is unsuitable for NQR. However, if a small magnetic field (either static or varying) is applied, the precession frequencies of the two components are no longer equal in magnitude. Consequently, the two components no longer cancel and a nonzero signal can result when the total magnetization at a given precession frequency is sampled by the nuclear-induction pickup coil. In principle, a signal could be observed if only a static magnetic field were present. However, noise considerations preclude such a technique. The experimental method which has been used[1,2,4] involves the application of an audio-frequency, sinusoidally varying magnetic field, which shifts the precession frequencies of the two components relative to each other (splits the quadrupole energy levels in the quantum sense) and also allows the use of phase-sensitive detection and amplification. As Robinson[2] points out, the nuclear-induction method gives greater signal-to-noise ratios than more conventional NQR techniques.

---

[1] R. R. Haering and G. M. Volkoff, Can. J. Phys. **34**, 577 (1956).

[2] L. B. Robinson, Can. J. Phys. **35**, 1344 (1957); **36**, 1295 (1958).

[3] H. Hartmann, M. Fleissner, and H. Sillescu, Naturwiss. **50**, 591 (1963); Theoret. Chem. Acta **2**, 63 (1964); H. Hartmann and H. Sillescu, *ibid.* **2**, 371 (1964).

[4] L. O. Anderson and W. G. Proctor, Varian AG. AID Application Bulletin No. 3.1.16.7.65, 1965 (unpublished); W. Proctor and K. Lee Varian Technical Information Bulletin, 1965 (unpublished), p. 6.

[5] G. W. Smith, Bull. Am. Phys. Soc. **11**, 221 (1966).

[6] T. P. Das and E. L. Hahn, *Nuclear Quadrupole Resonance Spectroscopy* (Academic Press Inc., New York, 1956), p. 83.

[7] D. J. E. Ingram, *Spectroscopy at Radio and Microwave Frequencies* (Philosophical Library, New York, 1956), p. 253.

[8] R. Livingston, in *Methods of Experimental Physics*, edited by D. Williams (Academic Press Inc., New York, 1962), Vol. 3, p. 507.

[9] Ref. 6, p. 74ff.

[10] M. Bloom, E. L. Hahn, and B. Herzog, Phys. Rev. **97**, 1699 (1955).

[11] H. G. Dehmelt, Am. J. Phys. **22**, 110 (1954).

[12] H. Kopfermann, *Nuclear Moments* (Academic Press Inc., New York, 1958), p. 327.

Most previous NQR work has dealt with line position measurement and relaxation effects, with less attention given to line shapes. This is perhaps partly due to the fact that some experimental methods introduce line-shape distortions (e.g., super-regenerative devices, Zeeman modulation techniques). Fourier analysis of free induction decays[10] can, of course, yield information on line shapes. Negita[13] has given a theory of Zeeman-modulated signal shapes for Lorentzian and Gaussian lines, and Morino and Toyama[14] have considered the Zeeman effect for NQR of spin $\frac{3}{2}$ nuclei in a powder. In the present work we shall present a semiclassical theory of the method of NQR by induction. We shall see that, at least in certain cases, the induction method yields no line-shape distortion, neglecting any possible effects of spin quenching.[15] The effect of spin quenching should be no larger for the induction method than for any other method using magnetic modulation. If H_z is the applied magnetic field and H_L the local dipolar field, the condition favorable to quenching is $\mu(H_z+H_L)\lesssim\eta eqQ$, so that in the present case we do not expect the magnetic field to produce sizable quenching of the spin-1–spin-1 interaction. Quenching of the spin-$\frac{1}{2}$–spin-1 interaction should be zero for $\eta=0$; and for hexamethylenetetramine, the test sample used in this work, $\frac{1}{2}$–1 is the dominant line-broadening mechanism. At any rate, we are primarily interested, in the present paper, in the effect of experimental parameters on a line broadened by unspecified interactions. Quenching can, of course, be important to the present interpretation if the degree of quenching is modulated by the magnetic field used in the experiment. However, like Negita,[13] we shall assume that the magnetic field does not influence the various natural line-broadening interactions. Inasmuch as theory and experiment give reasonable agreement, this seems to be a fair assumption.

The theory will be derived under three other major assumptions: (1) nuclear spin $I=1$; (2) an electric field gradient cylindrically symmetric about the z axis ($\eta=0$); and (3) relaxation processes parallel and transverse to the z axis, each describable by single relaxation times T_1 and T_2. The effect of these assumptions will be discussed in some detail and a qualitative extension to $I>1$, $\eta>0$ made. The assumption of a single T_2 automatically builds into the theory a Lorentzian line shape which produces an effect on the agreement between theory and experiment. However, the inclusion of a single relaxation time T_2 is the simplest way in which to take account of line-broadening effects, and the assumption of Lorentzian lines is not so restrictive as to prevent at least qualitative (and often quantitative) agreement between theory and experiment. It was deemed too difficult to build in the more realistic Gaussian line shape; furthermore, it became apparent that the slight improvement in agreement with experiment would hardly be worth the extra effort.

We shall obtain expressions for the NQR induction line shapes, the dependence of the slow-passage absorption mode signal upon static and modulation magnetic field, and the effect of rf field upon both the absorption and dispersion modes. The theory will be extended to single-coil (absorption-type) experiments. But first let us review briefly in Sec. II a slightly modified version of the work of Bloom, Robinson, and Volkoff,[16] who have derived modified Bloch equations and have given a slow-passage solution.[17] A special case of their solution will be the point of departure in our derivation.

II. NQR BLOCH EQUATIONS AND THEIR SLOW-PASSAGE SOLUTION

A. Derivation

Inasmuch as BRV were interested in covering the range of cases from pure NQR to NMR with quadrupolar perturbations, they considered the most general case: that for which the nuclear-spin wave functions are not necessarily characteristic of any particular spin component (say I_z). Hence, none of the matrix elements $\langle 1|I_x|2\rangle$, $\langle 1|I_y|2\rangle$, and $\langle 1|I_z|2\rangle$ between levels 1 and 2 are identically zero. We shall be interested in the case of pure NQR in only a weak magnetic perturbation; therefore, let us define the Z axis as the axis of quantization of the quadrupolar system. Hence, $\langle 1|I_z|2\rangle=0$. In addition, we shall be particularly interested in the case for axial symmetry ($\eta=0$) of a spin-1 system, which corresponds to the ^{14}N resonance in hexamethylenetetramine.[18] The axially symmetric case for other spins is easily obtained by an extension. We shall also discuss the nonaxial cases ($\eta\neq0$).

Let us, with BRV, consider the two level system illustrated in Fig. 1. For $I=1$ this corresponds to considering the $m=0$ plus one of the degenerate $m=\pm1$ levels. In the classical picture this is equivalent to considering one of the two oppositely precessing components of magnetization at a time. For an unperturbed system, the ith level has wave function ψ_i and energy E_i. The unperturbed Hamiltonian is $\mathcal{H}_0$, and the wave function is characteristic of I_z.[19] (thus $\mathcal{H}_0\psi_i=E_i\psi_i$, and $I_z\psi_i=m_i\psi_i$). $\mathcal{H}_0$ may be the Hamiltonian for either

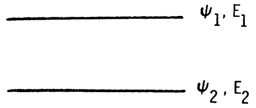

FIG. 1. Energy levels and wave functions.

---

[13] H. Negita, J. Chem. Phys. 44, 1734 (1966).

[14] Y. Morino and M. Toyama, J. Chem. Phys. 35, 1289 (1961).

[15] G. W. Leppelmeier and E. L Hahn, Phys. Rev. 141, 724. 1966.

[16] M. Bloom. L. B. Robinson, and G. M. Volkoff, Can. J. Phys. 36, 1286 (1958), hereinafter referred to as BRV.

[17] M. Bloom, E. L. Hahn, and B. Herzog (Ref. 10), had previously given explicit Bloch-like NQR equations.

[18] G. D. Watkins and R. V. Pound, Phys. Rev. 85, 1062 (1952).

[19] As pointed out above, BRV do not make this latter assumption since they are interested in the more general case.

a pure quadrupole interaction or quadrupole interaction plus magnetic perturbation.

If the system is perturbed by the interaction of an rf magnetic field $H_{\rm rf}$ with the nuclear moments (Hamiltonian $\mathcal{H}_1(t)=\gamma\hbar\mathbf{I}\cdot\mathbf{H}_{\rm rf}$, transitions between levels 1 and 2 are stimulated, and the equilibrium population of the levels is disturbed. The new situation can be described by a wave function $\psi=a\psi_1+b\psi_2$, where all the time dependence is contained in the coefficients a and b. Substitution in the time-dependent Schrödinger equation,

$$i\hbar\dot{\psi}=(\mathcal{H}_0+\mathcal{H}_1)\psi,$$

yields equations for $\dot{a}$ and $\dot{b}$ in terms of a, b, E_1, E_2, and matrix elements $P=\langle 1|I_x|2\rangle$ and $iS=\langle 1|I_y|2\rangle$. (The matrix element $T=\langle 1|I_z|2\rangle=0$ under our assumption that $I_z\psi_i=m_i\psi_i$). We define the average spin components as $\bar{I}_x=\langle\psi^*|I_x|\psi\rangle$ and $\bar{I}_y=\langle\psi^*|I_y|\psi\rangle$ and the population difference between the levels as $n=a^*a-b^*b$. The time derivatives of these three quantities, together with the equations in $\dot{a}$ and $\dot{b}$, yield Bloch-like equations[20] for $\dot{\bar{I}}_x$, $\dot{\bar{I}}_y$, and $\dot{n}$. The assumption that the classical magnetizations are proportional to the average spin components ($M_x=\gamma\hbar\bar{I}_x$, $M_y=\gamma\hbar\bar{I}_y$, and $M_z=\gamma\hbar\bar{I}_z=\gamma\hbar n/2$) plus the inclusion of single transverse and longitudinal relaxation times yields Bloch equations[10,16] which are applicable to NQR as well as to NMR. For a single precessing component, these are

$$\dot{M}_x=\frac{P}{S}\omega_0M_y-4\gamma PSH_yM_z-\frac{M_x}{T_2}, \tag{1a}$$

$$\dot{M}_y=4\gamma PSH_xM_z-\frac{S}{P}\omega_0M_x-\frac{M_y}{T_2}, \tag{1b}$$

$$\dot{M}_z=\gamma\left[\frac{S}{P}H_yM_x-\frac{P}{S}H_xM_y\right]+\frac{M_0-M_z}{T_1}, \tag{1c}$$

where $\omega_0=(E_1-E_2)/\hbar$, H_x and H_y are the X and Y components of the rf field, T_1 and T_2 are the relaxation times, γ is the gyromagnetic ratio, and M_0 is the equilibrium value of M_z.

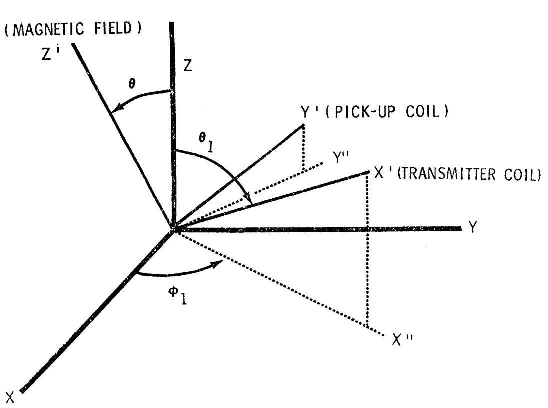

FIG. 2. Spin and laboratory (lab) coordinate systems.

It is important to recall that the XYZ axes are tied to the nuclear-spin system, with the Z axis defined by the direction of the principle internal electric field gradient. Hence, the Z axis is the quantization axis. Equations (1) reflect this since they represent magnetization precessing about Z. Furthermore, because of our definition of the Z axis, H_z, the Z component of the rf magnetic field, does not appear in the equations. We see that, because of the factor ω_0 in Eqs. (1a) and (1b), $|\dot{M}_x|$ and $|\dot{M}_y|\gg|\dot{M}_z|$. Consequently any nuclear induction signal will be due mainly to $\dot{M}_x$ and $\dot{M}_y$.

B. Slow-Passage Solution

In order to solve the Bloch equations, we must define a laboratory coordinate system. In Fig. 2 the laboratory (lab) axes are labeled $X'Y'Z'$ and the spin axes XYZ. An rf magnetic field $H_{\rm rf}$ of intensity $2H_1\cos\omega t$ is applied along the X' axis, and any applied static or audio frequency magnetic field along the Z' axis. The nuclear-induction pickup coil is coaxial with Y'. The angles for X' are defined as in BRV. X'' and Y'' mark the intersection of the $X'Z$ and $Y'Z$ planes with the XY plane.

A number of methods for solution of the Bloch equations are open to us. One is outlined by BRV, and solutions for $\bar{I}_x$, $\bar{I}_y$, and n are given. Their method of solution, being for a more general case than ours, is of necessity more difficult algebraically.

We shall resolve the rf field into two oppositely rotating components in the XY plane, the Z component being unimportant, as seen above. Then we shall consider the interaction of each rf component with that magnetization component precessing with the same sense. The total magnetization in the XY plane will then be the sum of the magnetizations of the two precessing components. This total magnetization can be resolved along the X and Y axes as $M_x^{\rm total}$ and $M_y^{\rm total}$. The magnetization, $M_{y'}$, along the pickup coil will be found from $M_x^{\rm total}$, $M_y^{\rm total}$, and the proper direction cosines, $\cos(X,Y')$ and $\cos(Y,Y')$.

The first steps in the solution are exactly analogous to those in the Bloch "slow-passage" NMR case,[20] but we shall sketch them briefly in order to establish a basis and introduce notation for what is to follow: i.e. the derivation of NQR induction line shapes and their dependence on experimental parameters.

We resolve $H_{\rm rf}$ into counterclockwise and clockwise rotating components (in the XY plane):

ccw (looking along Z): $H_{x''}=H_1\sin\theta_1\cos\omega t$; $H_{y''}=-H_1\sin\theta_1\sin\omega t$,

cw (looking along Z): $H_{x''}=H_1\sin\theta_1\cos\omega t$; $H_{y''}=H_1\sin\theta_1\sin\omega t$.

In order to work with the Bloch equations, we further

---

[20] F. Bloch, Phys. Rev. **70**, 460 (1946).

resolve H_{rf} along X and Y:

$$\text{ccw:}\quad H_x=\alpha\cos\omega t+\xi\sin\omega t;\quad H_y=\xi\cos\omega t-\alpha\sin\omega t\,,\tag{2a}$$

$$\text{cw:}\quad H_x=\alpha\cos\omega t-\xi\sin\omega t;\quad H_y=\xi\cos\omega t+\alpha\sin\omega t\,,\tag{2b}$$

where

$$\alpha=H_1\sin\theta_1\cos\varphi_1\quad\text{and}\quad\xi=H_1\sin\theta_1\sin\varphi_1.\tag{2c}$$

1. Counterclockwise Component $(1\leftrightarrow 0)$

Let us consider first the $1\leftrightarrow 0$ transition. We see[10] that this transition is associated with the ccw case. In the presence of a small magnetic field H along Z' the precession frequency for this component goes[21] from ω_0 to $\omega_0-\Omega\cos\theta$, where $\Omega=\gamma H$. (Note: the sign of H is not crucial in what follows. It is only essential that the $1\leftrightarrow 0$ and $-1\leftrightarrow 0$ frequencies be shifted in opposite senses.) Furthermore, for $I=1$, the ccw component corresponds to[22] $P=\sqrt{2}/2$ and $S=\sqrt{2}/2$.

Following the Bloch slow-passage procedure, we let

$$M_x=u\cos\omega t-v\sin\omega t\,,\quad M_y=-(u\sin\omega t+v\cos\omega t)\,,\tag{3}$$

where $\dot{u}=\dot{v}=\dot{M}_z\cong 0$. Thus in the slow-passage picture the time dependence of the magnetization is dominated by the sinusoidal terms. This fact eliminates the necessity of differentiating our result for $M_{y'}$ in the final result since time differentiation merely multiplies the magnetization by ω and shifts its phase. The use of paddles in the induction experimental method allows us to measure either the in-phase or out-of-phase component of magnetization.

Substitution of Eqs. (2a) and (3) into (1) with $P=S=\sqrt{2}/2$, yields (for $\Omega=0$)

$$\begin{aligned}M_x&=\frac{2\gamma M_0T_2[(\alpha T_2\Delta\omega-\xi)\cos\omega t+(\alpha+\xi T_2\Delta\omega)\sin\omega t]}{K}\,,\\ M_y&=\frac{2\gamma M_0T_2[(\alpha+\xi T_2\Delta\omega)\cos\omega t+(\xi-\alpha T_2\Delta\omega)\sin\omega t]}{K}\,,\end{aligned}\tag{4}$$

where $\Delta\omega=\omega_0-\omega$ and

$$K=1+\Delta\omega^2T_2^2+2\gamma^2H_1^2T_1T_2\sin^2\theta_1.$$

2. Clockwise Component $(-1\leftrightarrow 0)$

For this component a small magnetic field along Z' produces a frequency shift from ω_0 to $\omega_0+\Omega\cos\theta$. Also, for $I=1$, $P=\sqrt{2}/2$ and $S=-\sqrt{2}/2$. We take

$$M_x=u\cos\omega t-v\sin\omega t;\quad M_y=u\sin\omega t+v\cos\omega t.\tag{5}$$

The expressions for the u and v modes of the cw component (with $\Omega=0$) will not necessarily be identical to those for the ccw component since the lab axes are not necessarily coincident with the spin axes.

The Bloch equations yield

$$\begin{aligned}M_x&=\frac{2\gamma M_0T_2[(\alpha T_2\Delta\omega+\xi)\cos\omega t+(\alpha-\xi T_2\Delta\omega)\sin\omega t]}{K}\,,\\ M_y&=\frac{2\gamma M_0T_2[(\xi T_2\Delta\omega-\alpha)\cos\omega t+(\xi+\alpha T_2\Delta\omega)\sin\omega t]}{K}\,.\end{aligned}\tag{6}$$

These same expressions could have been obtained from Eqs. (16) of BRV or from solutions of the Bloch equations along the $X''Y''$ axes (see Fig. 2).

III. THE INDUCED VOLTAGE IN THE PICKUP COIL

We can now use Eqs. (4) and (6) to derive expressions for the component $M_{y'}$ of precessing magnetization along the pickup coil axis (Y') .The induced voltage is the proportional to $dM_{y'}/dt$, but, as we have already seen, the differentiation process merely introduces a phase shift and a factor of ω. Thus, it will suffice to solve for $M_{y'}$.

The basic equations are

$$M_{y'}=M_x^{\mathrm{total}}\cos(X,Y')+M_y^{\mathrm{total}}\cos(Y,Y')\,,\tag{7}$$

where

$$M_x^{\mathrm{total}}=M_x(1\leftrightarrow 0)+M_x(-1\leftrightarrow 0)\,,$$

and

$$M_y^{\mathrm{total}}=M_y(1\leftrightarrow 0)+M_y(-1\leftrightarrow 0)\,.$$

Let us consider first the case for a single crystal of equivalent nuclei in the absence of saturation effects. Our definition of equivalent nuclei, in addition to the usual factors, shall include the requirement that the directions of the electric field gradient be the same at each nuclear site, in order that the lab axes make the same angles with each nucleus' spin axes. (Hence, in a single crystal of hexamethylenetetramine, although all the ^{14}N atoms are chemically and structurally equivalent, their nuclei are not equivalent, as far as we are concerned, because of the tetrahedral arrangement of the field-gradient directions in a single molecule.[23])

A. Single Crystal, $Z'\|Z$, Equivalent Nuclei

The signal for a single crystal is maximum if Z and Z, coincide. In this case, for small magnetic field, the central precession frequencies become shifted from ω_0 to $\omega_\pm$:

$$\begin{aligned}\text{ccw:}\quad \omega_-&=\omega_0-\Omega\,,\\ \text{cw:}\quad \omega_+&=\omega_0+\Omega\,.\end{aligned}\tag{8}$$

Also, since $\theta_1=\pi/2$, we have that $\alpha=H_1\cos\varphi_1$ and $\xi=H_1\sin\varphi_1$. If we let $C=2\gamma H_1M_0T_2$, Eqs. (4) and (6)

---

[21] Reference 6, p. 8ff.

[22] E. U. Condon, in *Handbook of Physics*, edited by E. U. Condon and H. Odishaw (McGraw-Hill Book Company, Inc., New York, 1958), pp. 2–44.

[23] S. Alexander and A. Tzalmona, Phys. Rev. **138**, A845 (1965).

become

ccw$(1\leftrightarrow 0)$

$$M_x=\frac{C}{1+(\Delta\omega-\Omega)^2T_2^2}\{[(\Delta\omega-\Omega)T_2\cos\varphi_1-\sin\varphi_1]\times\cos\omega t+[\cos\varphi_1+(\Delta\omega-\Omega)T_2\sin\varphi_1]\sin\omega t\},$$

$$M_y=\frac{C}{1+(\Delta\omega-\Omega)^2T_2^2}\{[(\Delta\omega-\Omega)T_2\sin\varphi_1+\cos\varphi_1]\times\cos\omega t+[\sin\varphi_1-(\Delta\omega-\Omega)T_2\cos\varphi_1]\sin\omega t\};$$

cw$(-1\leftrightarrow 0)$

$$M_x=\frac{C}{1+(\Delta\omega+\Omega)^2T_2^2}\{[(\Delta\omega+\Omega)T_2\cos\varphi_1+\sin\varphi_1]\times\cos\omega t+[\cos\varphi_1-(\Delta\omega+\Omega)T_2\sin\varphi_1]\sin\omega t\},$$

$$M_y=\frac{C}{1+(\Delta\omega+\Omega)^2T_2^2}\{[(\Delta\omega+\Omega)T_2\sin\varphi_1-\cos\varphi_1]\times\cos\omega t+[\sin\varphi_1+(\Delta\omega+\Omega)T_2\cos\varphi_1]\sin\omega t\}.$$

Using these relations we derive $M_{y'}$ from Eqs. (7), where $\cos(X,Y')=-\sin\varphi_1$ and $\cos(Y,Y')=\cos\varphi_1$ for the present alignment. The nuclear induction probe paddles allow us to tune either to the $\sin\omega t$ or $\cos\omega t$ term of $M_{y'}$. Thus the detected voltage from the receiver is proportional to the coefficient either of the $\cos\omega t$ term or of the $\sin\omega t$ term. Let us consider first the $\cos\omega t$ term, which, along Y', corresponds to the absorption mode.

1. Absorption or V Mode (cosωt Term)

After a few algebraic operations, Eqs. (7) yield for the coefficient of the $\cos\omega t$ term

$$M_{y'}{}^{\cos}=\frac{4CT_2{}^2\Omega\Delta\omega}{[1+(\Delta\omega+\Omega)^2T_2{}^2][1+(\Delta\omega-\Omega)^2T_2{}^2]},\tag{9}$$

which in the limit of small Ω becomes

$$M_{y'}{}^{\cos}=\frac{4CT_2{}^2\Omega\Delta\omega}{(1+\Delta\omega^2T_2{}^2)^2}.\tag{10}$$

This expression is the derivative of a Lorentzian absorption mode[24] signal, $1/(1+\Delta\omega^2T_2{}^2)$. The linewidth between derivative extrema is $\delta\omega=2/(\sqrt{3}T_2)$. This result is not too surprising since the Bloch picture automatically builds in a Lorentzian line shape, and since the differencing process yields a derivative. For small Ω the signal amplitude is proportional to the applied magnetic field.

2. Dispersion or U Mode (sinωt Term)

In a similar way the expression for the dispersion mode[25] is

$$M_{y'}{}^{\sin}=\frac{2CT_2\Omega(1-\Delta\omega^2T_2{}^2+\Omega^2T_2{}^2)}{[1+(\Delta\omega+\Omega)^2T_2{}^2][1+(\Delta\omega-\Omega)^2T_2{}^2]},\tag{11}$$

which in the limit of small Ω becomes

$$M_{y'}{}^{\sin}=\frac{2CT_2\Omega(1-\Delta\omega^2T_2{}^2)}{(1+\Delta\omega^2T_2{}^2)^2}.\tag{12}$$

This equation is the derivative of a Lorentzian dispersion mode signal, $\Delta\omega T_2/(1+\Delta\omega^2T_2{}^2)$. Again the signal is proportional to Ω for small fields.

B. Polycrystalline Sample

In order to find $M_{y'}$ for a polycrystalline sample, it is necessary to describe the relationship between the laboratory and spin coordinates by means of Euler angles. This means that we shall also need equations relating θ_1 and φ_1 to the Euler angles. Figure 3 shows the Euler angles[26] φ, θ, and ψ and, in parentheses, the unit vectors $\hat{\imath}$, $\hat{\jmath}$, $\hat{k}$ for the spin (XYZ) axes and $\hat{l}$, $\hat{m}$, $\hat{n}$ for the lab ($X'Y'Z'$) axes. Using the relation (see Fig. 2)

$$\hat{l}=\cos\theta_1\hat{k}+\sin\theta_1\cos\varphi_1\hat{\imath}+\sin\theta_1\sin\varphi_1\hat{\jmath},$$

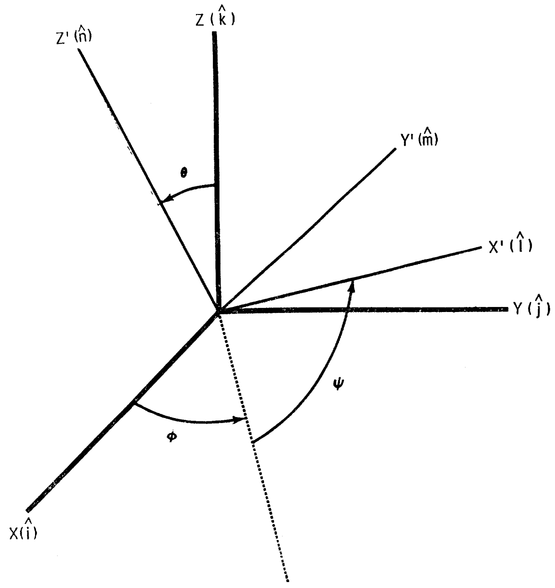

FIG. 3. Euler angles relating spin and laboratory (lab) coordinates.

---

[24] Capital V is used to avoid confusion with the v mode of Sec. II.

[25] Capital U is used to avoid confusion with the u mode of Sec. II.

[26] Reference 22, p. 2–5.

and the table of Condon,[26] we get

$$\hat{l}\cdot\hat{\imath}=\sin\theta_1\cos\varphi_1=\cos\varphi\cos\psi-\sin\varphi\sin\psi\cos\theta, \tag{13a}$$

$$\hat{l}\cdot\hat{\jmath}=\sin\theta_1\sin\varphi_1=\sin\varphi\cos\psi+\cos\varphi\sin\psi\cos\theta, \tag{13b}$$

$$\hat{l}\cdot\hat{k}=\cos\theta_1=\sin\theta\sin\psi,$$

or (13c)

$$\sin^2\theta_1=1-\sin^2\theta\sin^2\psi.$$

Note that Eqs. (13a) and (13b) convert Eqs. (2c) for α and ξ directly to expressions involving Euler angles. In addition Eq. (13c) converts the saturation term $2\gamma^2H_1{}^2T_1T_2\sin^2\theta_1$ of Eq. (4) to Euler angles. Also important is the fact that the Euler angle θ of Fig. 3 equals the polar angle θ for Z' in Fig. 2.

Use of the Condon table[26] also gives us expressions for the direction cosines:

$$\begin{aligned}\cos(X,Y')&=\hat{m}\cdot\hat{\imath}=-\cos\varphi\sin\psi-\sin\varphi\cos\psi\cos\theta,\\ \cos(Y,Y')&=\hat{m}\cdot\hat{\jmath}=-\sin\varphi\sin\psi+\cos\varphi\cos\psi\cos\theta.\end{aligned} \tag{14}$$

We recall that Eqs. (8) for a polycrystal are

$$\omega_\pm=\omega_0\pm\Omega\cos\theta. \tag{15}$$

Further, with $C=2\gamma H_1M_0T_2$ and $s=1+2\gamma^2H_1{}^2T_1T_2\times\sin^2\theta_1=1+2\gamma^2H_1{}^2T_1T_2(1-\sin^2\theta\sin^2\psi)$, Eqs. (4) and (6) become

ccw:

$$M_x=\frac{C[\{(\Delta\omega-\Omega\cos\theta)T_2\sin\theta_1\cos\varphi_1-\sin\theta_1\sin\varphi_1\}\cos\omega t+\{\sin\theta_1\cos\varphi_1+(\Delta\omega-\Omega\cos\theta)T_2\sin\theta_1\sin\varphi_1\}\sin\omega t]}{s+(\Delta\omega-\Omega\cos\theta)^2T_2{}^2},$$

$$M_y=\frac{C[\{(\Delta\omega-\Omega\cos\theta)T_2\sin\theta_1\sin\varphi_1-\sin\theta_1\cos\varphi_1\}\cos\omega t+\{\sin\theta_1\sin\varphi_1-(\Delta\omega-\Omega\cos\theta)T_2\sin\theta_1\cos\varphi_1\}\sin\omega t]}{s+(\Delta\omega-\Omega\cos\theta)^2T_2{}^2};$$

cw:

$$M_x=\frac{C[\{(\Delta\omega+\Omega\cos\theta)T_2\sin\theta_1\cos\varphi+\sin\theta_1\sin\varphi_1\}\cos\omega t+\{\sin\theta_1\cos\varphi_1-\sin\theta_1\sin\varphi_1(\Delta\omega+\Omega\cos\theta)T_2\}\sin\omega t]}{s+(\Delta\omega+\Omega\cos\theta)^2T_2{}^2},$$

$$M_y=\frac{C[\{(\Delta\omega+\Omega\cos\theta)T_2\sin\theta_1\sin\varphi_1-\sin\theta_1\cos\varphi_1\}\cos\omega t+\{(\Delta\omega+\Omega\cos\theta)T_2\sin\theta_1\cos\varphi_1+\sin\theta_1\sin\varphi_1\}\sin\omega t]}{s+(\Delta\omega+\Omega\cos\theta)^2T_2{}^2}.$$

These equations, plus Eqs. (7), (13), and (14), allow us to calculate $M_{y'}$. The absorption and dispersion signals for a randomly oriented crystallite can be found from the coefficients of $\cos\omega t$ and $\sin\omega t$ in the equation for $M_{y'}$. The signal for a polycrystalline sample is then obtained by averaging over all angles. We consider the $\cos\omega t$ term first.

1. *Absorption or V Mode* (*cosωt Term*)

After several algebraic steps the coefficient of $\cos\omega t$ in the expression for $M_{y'}$ becomes

$$M_{y'}{}^{\cos}=\frac{2C\Delta\omega T_2[-A\sin\psi\cos\psi\sin^2\theta+2T_2\Omega\cos^2\theta]}{[s+(\Delta\omega+\Omega\cos\theta)^2T_2{}^2][s+(\Delta\omega-\Omega\cos\theta)^2T_2{}^2]}, \tag{16}$$

where $A=s+(\Delta\omega^2-\Omega^2\cos^2\theta)T_2{}^2$.

Note that there is no dependence on the Euler angle φ in Eq. (16). This is important because it simplifies the averaging process for a polycrystal. Since the Euler angle θ equals the polar angle θ and since the Z' axis is normal to the plane containing ψ, we can treat ψ as an azimuthal angle and average $M_{y'}$ over angle using

$$\bar{M}_{y'}=\frac{1}{4\pi}\int_0^\pi\int_0^{2\pi}M_{y'}\sin\theta d\psi d\theta. \tag{17}$$

Let us consider saturation effects and magnetic field effects separately. Therefore, for the present we assume $2\gamma^2H_1{}^2T_1T_2\ll1$ or $s\approx1$ and investigate magnetic field effects only. Saturation effects will be considered in a separate section of this paper.

a. $s=1$, *Ω small.* The case of small magnetic field is important since it is expected to yield an experimental line which is a derivative of the true NQR signal. For Ω small and $s=1$, Eq. (16) becomes

$$M_{y'}{}^{\cos}=\frac{2C\Delta\omega T_2[-A\sin\psi\cos\psi\sin^2\theta+2T_2\Omega\cos^2\theta]}{[1+\Delta\omega^2T_2{}^2]^2}. \tag{16a}$$

When this is averaged over ψ using Eq. (17), the term in $\sin\psi\cos\psi$ goes to zero. Thus the polycrystalline signal becomes

$$\bar{M}_{y'}{}^{\cos}=\frac{4CT_2{}^2\Omega\Delta\omega}{3(1+\Delta\omega^2T_2{}^2)^2}. \tag{18}$$

This expression is $\frac{1}{3}$ the corresponding expression for a single crystal with optimum orientation (Eq. 10). This result is reasonable, for if Ω were aligned along X or Y the signal would be zero. Hence the average signal, in a simple picture, is $(0+0+1)/3$ times the signal for Ω along Z. Equation (18) also contains the important result that for small Ω, the polycrystalline signal shape is exactly the same as that of a single crystal. Because of the tetrahedral distribution of field-gradient directions in a single crystal of hexamethylenetetramine, the intensity of the single-crystal induction signal for this compound is probably approximated by the polycrystal result.

In Eqs. (16) and (16a) for a single crystal with θ not equal to 0 or π (i.e. Z not parallel to Z'), the term in $\sin\psi\,\cos\psi$ predicts a contribution to the signal even for $\Omega=0$. The existence of this term is a consequence of the nature of the derivation and has no physical meaning for $\Omega=0$ due to the neglect of the random orientation of the local dipolar fields.

b. $s=1$, Ω *unrestricted.* Consideration of this case describes how a magnetic field distorts the signal shape. Inasmuch as experiments usually deal with the absorption mode, we shall investigate in the rest of this section the field effect for this mode only.

Once again the $\sin\psi\,\cos\psi$ term of Eq. (16) averages to zero. We then have

$$\bar{M}_{y'}{}^{\cos}=2C\Delta\omega\Omega T_2{}^2\int_0^\pi\frac{\cos^2\theta\,\sin\theta d\theta}{[1+(\Delta\omega-\Omega\,\cos\theta)^2T_2{}^2][1+(\Delta\omega+\Omega\,\cos\theta)^2T_2{}^2]}. \tag{19}$$

This integral is soluble in closed form. Letting

$$\beta=\Delta\omega T_2 \qquad \text{and} \qquad \epsilon=\Omega T_2, \tag{20}$$

we have

$$\begin{aligned}\bar{M}_{y'}{}^{\cos}&=\frac{2C\beta}{\epsilon^2}\int_{-\epsilon}^{\epsilon}\frac{x^2dx}{[1+(\beta+x)^2][1+(\beta-x)^2]}\\&=\frac{C}{2\epsilon^2}\left[\ln\frac{1+(\beta-\epsilon)^2}{1+(\beta+\epsilon)^2}+2\beta\{\tan^{-1}(\beta+\epsilon)-\tan^{-1}(\beta-\epsilon)\}\right].\end{aligned} \tag{21}$$

For ϵ small, the numerical solution of Eq. (21) as a function of β is the Lorentzian curve of Eq. (18). If ϵ, the magnetic field parameter, is constant, Eq. (21) represents a constant signal amplitude. If ϵ contains a term which varies with time t as $\epsilon_m\,\cos\omega_mt$ ($\omega_m\ll\omega_0$), $\bar{M}_{y'}{}^{\cos}$ is a function of time with sizable contributions at the harmonics of the modulation frequency ω_m. In actual practice, a constant magnetic field alone is not used because of signal-to-noise problems. Instead, a modulating field is used and only the signal component at the fundamental modulation frequency detected. We shall postpone further discussion of this aspect of the problem and the related calculations until Sec. IV.

The linewidth $\delta\omega$ between slope extrema (rad/sec) is an important experimental parameter. To determine $\delta\omega$, we shall need the solutions to the expression $d\bar{M}_{y'}{}^{\cos}/d\beta=0$. Equation (21) yields

$$\frac{d\bar{M}_{y'}{}^{\cos}}{d\beta}=\frac{C}{\epsilon^2}\left[\frac{-2\epsilon(1+\epsilon^2+\beta^2)}{[1+(\beta-\epsilon)^2][1+(\beta+\epsilon)^2]}+\tan^{-1}(\beta+\epsilon)-\tan^{-1}(\beta-\epsilon)\right]. \tag{22}$$

Both Eqs. (21) and (22) will be further applied in the discussion of modulation effects.

2. *Dispersion or U Mode (sinωt Term)*

The dispersion mode, as obtained from the coefficient of the $\sin\omega t$ term, is

$$M_{y'}{}^{\sin}=\frac{2C[\Omega T_2\{s-(\Delta\omega^2-\Omega^2\,\cos^2\theta)T_2{}^2\}\,\cos^2\theta-\{s+(\Delta\omega^2+\Omega^2\,\cos^2\theta)T_2{}^2\}\,\sin^2\theta\,\sin\psi\,\cos\psi]}{[s+(\Delta\omega+\Omega\,\cos\theta)^2T_2{}^2][s+(\Delta\omega-\Omega\,\cos\theta)^2T_2{}^2]}. \tag{23}$$

Once again the φ dependence has disappeared, and the ψ-dependent terms average to zero.

c. $s=1$, Ω *small.* For $s=1$ and Ω small, Eq. (23) becomes

$$M_{y'}{}^{\sin}=\frac{2C[\Omega T_2(1-\Delta\omega^2T_2{}^2)\,\cos^2\theta-(1+\Delta\omega^2T_2{}^2)\,\sin^2\theta\,\sin\psi\,\cos\psi]}{(1+\Delta\omega^2T_2{}^2)^2}, \tag{24}$$

which averages to give

$$\bar{M}_{y'}{}^{\sin}=\frac{2CT_2\Omega(1-\Delta\omega^2T_2^2)}{3(1+\Delta\omega^2T_2^2)^2}. \tag{25}$$

As for the absorption mode, the polycrystalline signal is $\frac{1}{3}$ the optimum signal-crystal signal, when Ω is small.

IV. THEORETICAL ABSORPTION MODE SIGNAL FOR PHASE-SENSITIVE DETECTION TECHNIQUE. MAGNETIC FIELD EFFECTS

Let us now include the details of the experimental method in order to calculate the absorption-mode line shape and linewidth for modulations of an arbitrary amplitude. We assume the rf field to be nonsaturating ($s=1$). As we shall see, increased modulation amplitude produces broadening of the NQR induction signal. Modulation effects for NMR have been previously discussed.[27–29]

For the sake of generality, we shall consider our magnetic field to consist of both a static and a sinusoidal component. A phase-sensitive detector and lock-in amplifier unit rejects all portions of the detected signal from the induction pickup coil which are not of the same frequency and phase as the modulating magnetic field. In this and the following sections it will be convenient to consider the polycrystal sample first since our experiment dealt with a polycrystalline sample.

A. Polycrystalline Sample

In mathematical terms the total V-mode induction signal is described by Eq. (21) where the magnetic field contains collinear static and modulation terms

$$\epsilon=\epsilon_s+\epsilon_m\cos\omega_m t, \tag{26}$$

where $\epsilon_s=\Omega_sT_2=\gamma h_sT_2$ and $\epsilon_m=\Omega_mT_2=\gamma h_mT_2$, and the collinear static and modulating components of the magnetic field are h_s and h_m. If the detected signal due to the magnetization is expressed as a Fourier series

$$\bar{M}_{y'}=\sum_{n=0}^{\infty}a_n\cos n\omega_m t, \tag{27}$$

the recorded signal is proportional to the coefficient a_1.[30] Then by the usual analysis,

$$a_1=\frac{1}{\pi}\int_{-\pi/\omega_m}^{\pi/\omega_m}\bar{M}_{y'}(\cos\omega_m t)(\omega_m dt)=\frac{1}{\pi}\int_{-\pi}^{\pi}\bar{M}_{y'}\cos\theta_m d\theta_m, \tag{28}$$

where $\theta_m=\omega_m t$. Use of Eq. (21) and the fact that $\bar{M}_{y'}\cos\theta_m$ is an even function of θ_m yields

$$a_1=\frac{c}{\pi}\int_0^{\pi}\frac{\cos\theta_m}{(\epsilon_s+\epsilon_m\cos\theta_m)^2}\left\{\ln\left[\frac{1+(\beta-\epsilon_s-\epsilon_m\cos\theta_m)^2}{1+(\beta+\epsilon_s+\epsilon_m\cos\theta_m)^2}\right]+2\beta[\tan^{-1}(\beta+\epsilon_s+\epsilon_m\cos\theta_m)-\tan^{-1}(\beta-\epsilon_s-\epsilon_m\cos\theta_m)]\right\}d\theta_m. \tag{29}$$

Similarly, to find the linewidth, it is necessary to solve the equation

$$\frac{da_1}{d\beta}=0=\frac{1}{\pi}\frac{d}{d\beta}\int_{-\pi}^{\pi}\bar{M}_{y'}\cos\theta_m d\theta_m=\frac{1}{\pi}\int_{-\pi}^{\pi}\frac{d\bar{M}_{y'}}{d\beta}\cos\theta_m d\theta_m, \tag{30}$$

where $d\bar{M}_{y'}/d\beta$ is given in Eq. (22).

Equations (29) and (30) have been solved numerically using a FORTRAN II computer program and an IBM 7094 computer. The results of the computations will be discussed and compared with experiment in Sec. VII.

B. Single Crystal

For an optimally oriented single crystal, Eqs. (9) and (28) give

$$a_1=\frac{8C}{\pi}\int_0^{\pi}\frac{\beta(\epsilon_s+\epsilon_m\cos\theta_m)\cos\theta_m d\theta_m}{[1+(\beta+\epsilon_s+\epsilon_m\cos\theta_m)^2][1+(\beta-\epsilon_s-\epsilon_m\cos\theta_m)^2]}. \tag{31}$$

One expects that, for ϵ_s and ϵ_m small, Eq. (31) will equal 3 times Eq. (29), and, indeed, the numerical calculations do yield this result. Single-crystal line widths were obtained from extremum values of a_1 in Eq. (31).

C. Second Moment

Since the present theory has built into it a Lorentzian line shape, for which the second moment, S, is infinite, we present no theoretical dependence of S on the magnetic field. However, the experimental second moment will be discussed later.

---

[27] O. E. Myers and E. J. Putzer, J. Appl. Phys. **30**, 1987 (1959); **37**, 458 (1966).

[28] H. Wahlquist, J. Chem. Phys. **35**, 1708 (1961); G. V. H. Wilson, J. Appl. Phys. **34**, 3276 (1963).

[29] G. W. Smith, J. Appl. Phys. **35**, 1217 (1964).

[30] E. R. Andrew, Phys. Rev **91**, 425 (1953).

V. RF FIELD EFFECTS—SATURATION THEORY

We shall now consider the effects of an rf field H_1 which is large enough to produce saturation. In addition, we shall restrict Ω to small values so that no signal distortion due to modulation occurs, Hence, we use Eqs. (16) and (23) with $\Omega \approx 0$ as starting points for discussion of the absorption and dispersion mode effects. Our considerations correspond roughly to case I of Bloembergen, Purcell, and Pound[31] for NMR ($\omega_m T_1 \ll 1$). However, since cases I and II of BPP are qualitatively similar, this treatment will suffice.

A. Absorption Mode, Polycrystal

For $\Omega T_2 \ll 1$ and $\sigma = 2\gamma^2 H_1^2 T_1 T_2$, Eq. (16) becomes

$$M_{y'}{}^{\cos} = \frac{2C\Delta\omega T_2[-(1-\sigma-\sigma\sin^2\theta\sin^2\psi+\Delta\omega^2 T_2^2)\sin\psi\cos\psi\sin^2\theta+2T_2\Omega\cos^2\theta]}{(1+\sigma-\sigma\sin^2\theta\sin^2\psi+\Delta\omega^2 T_2^2)^2}. \tag{32}$$

The first term on the right, being an odd function of ψ, integrates to zero in a polycrystalline average. Thus

$$\bar{M}_{y'}{}^{\cos} = \frac{C\Delta\omega T_2{}^2\Omega}{\pi}\int_0^{2\pi}\int_0^{\pi}\frac{\cos^2\theta\sin\theta d\theta d\psi}{(\kappa-\sigma\sin^2\theta\sin^2\psi)^2}, \tag{33}$$

where $\kappa = 1+\sigma+\Delta\omega^2 T_2^2$. This can be put into form approximating the familiar NMR result by factoring out κ^2 in the denominator:

$$\bar{M}_{y'}{}^{\cos} = \frac{C\Delta\omega T_2{}^2\Omega}{\pi(1+\sigma+\Delta\omega^2 T_2^2)^2}\int_0^{2\pi}\int_0^{\pi}\frac{\cos^2\theta\sin\theta d\theta d\psi}{[1-(\sigma/\kappa)\sin^2\theta\sin^2\psi]^2}. \tag{34}$$

Since $\sigma/\kappa < 1$, the factor $[1-\sigma(\sin^2\theta\sin^2\psi)/\kappa]^{-2}$ can be expressed by means of a series expansion. Integration of the first five terms of the resulting expression gives

$$\bar{M}_{y'}{}^{\cos} = \frac{4CT_2{}^2\Delta\omega\Omega}{3(1+\sigma+\Delta\omega^2 T_2^2)^2}\left[1+\frac{2}{5}\frac{\sigma}{\kappa}+\frac{9}{35}\left(\frac{\sigma}{\kappa}\right)^2+\frac{4}{21}\left(\frac{\sigma}{\kappa}\right)^3+\frac{5}{33}\left(\frac{\sigma}{\kappa}\right)^4+\cdots\right]. \tag{35}$$

In order to evaluate this expression at the extrema of the recorded (derivative) signal, we must know the dependence of the extremum position upon σ. Evaluation of this dependence from Eq. (35) would be tedious. However, for σ not too large, the first term in the series dominates. Under this assumption, we get $\Delta\omega T_2 \cong \pm((1+\sigma)/3)^{1/2}$ when $d\bar{M}_{y'}{}^{\cos}/d\beta = 0$. At this same point $\kappa \cong 4(1+\sigma)/3$ and $\sigma/\kappa \cong 3\sigma/[4(1+\sigma)]$. Thus, to a fair approximation, the dependence of signal strength at maximum slope upon rf becomes

$$(\bar{M}_{y'}{}^{\cos})_{\max} = \frac{\sqrt{3}\gamma M_0 T_2{}^2\Omega H_1}{2(1+\sigma)^{3/2}}\left[1+0.3\left(\frac{\sigma}{1+\sigma}\right)+0.145\left(\frac{\sigma}{1+\sigma}\right)^2+0.080\left(\frac{\sigma}{1+\sigma}\right)^3+0.047\left(\frac{\sigma}{1+\sigma}\right)^4\right]. \tag{36}$$

The $(1+\sigma)^{-3/2}$ dependence demonstrates the relationship to case I of BPP and is what one expects for the derivative maximum of a Bloch-like v-mode signal. Equation (36) is probably good to better than 10%. The next term in the brackets is $0.0299\,[\sigma/(1+\sigma)]^5$.

B. Dispersion Mode, Polycrystal

Similarly, for the dispersion signal, only the first term on the right of Eq. (23) contributes to the polycrystal signal. For $\Omega T_2 \approx 0$ we have

$$\bar{M}_{y'}{}^{\sin} = \frac{C\Omega T_2}{2\pi}\int_0^{\pi}\int_0^{2\pi}\frac{(1+\sigma-\sigma\sin^2\theta\sin^2\psi-\Delta\omega^2 T_2^2)\cos^2\theta\sin\theta d\psi d\theta}{(1+\sigma-\sigma\sin^2\theta\sin^2\psi+\Delta\omega^2 T_2^2)^2}.$$

Letting $\lambda = 1+\sigma-\Delta\omega^2 T_2^2$ and $\kappa = 1+\sigma+\Delta\omega^2 T_2^2$, we have

$$\bar{M}_{y'}{}^{\sin} = \frac{C\Omega T_2(1+\sigma-\Delta\omega^2 T_2^2)}{2\pi(1+\sigma+\Delta\omega^2 T_2^2)^2}\int_0^{\pi}\int_0^{2\pi}\frac{[1-(\sigma/\lambda)\sin^2\theta\sin^2\psi]\cos^2\theta\sin\theta d\psi d\theta}{[1-(\sigma/\kappa)\sin^2\theta\sin^2\psi]^2}.$$

---

[31] N. Bloembergen, E. M. Purcell, and R. V. Pound, Phys.Rev. 73, 679 (1948).

However, as is well known, the derivative of the dispersion signal is a maximum at $\Delta\omega=0$. Thus

$$(\bar{M}_{y'}{}^{\sin})_{\max}=\frac{C\Omega T_2}{2\pi(1+\sigma)}\int_0^{\pi}\int_0^{2\pi}\frac{\cos^2\theta\,\sin\theta d\psi d\theta}{[1-(\sigma/\kappa)\sin^2\theta\,\sin^2\psi]}. \tag{37}$$

Following a series expansion, Eq. (37) becomes

$$\begin{aligned}(\bar{M}_{y'}{}^{\sin})_{\max}&=\frac{2CT_2\Omega}{3(1+\sigma)}\left[1+\frac{1}{5}\frac{\sigma}{\kappa}+\frac{3}{35}\left(\frac{\sigma}{\kappa}\right)^2+\frac{1}{21}\left(\frac{\sigma}{\kappa}\right)^3+\frac{1}{33}\left(\frac{\sigma}{\kappa}\right)^4+\cdots\right]\\&=\frac{4\gamma H_1M_0T_2{}^2\Omega}{3(1+\sigma)}\left[1+0.2\left(\frac{\sigma}{1+\sigma}\right)+0.0857\left(\frac{\sigma}{1+\sigma}\right)^2+0.0476\left(\frac{\sigma}{1+\sigma}\right)^3+0.0303\left(\frac{\sigma}{1+\sigma}\right)^4+\cdots\right].\end{aligned} \tag{38}$$

The dominant $(1+\sigma)^{-1}$ dependence is exactly what one expects for the derivative maximum of a Bloch *u*-mode signal.

Equations (36) and (38) predict that, for $\sigma\approx0$, the peak-to-peak absorption mode signal should be 1.3 times the peak amplitude of the dispersion signal. In the spectra of Fig. 4, this ratio is about 1.4.

C. Single Crystal

For a single crystal, the dependence of the absorption mode signal on rf can be obtained directly from Eq. (32). Eq. (23) is easily modified to give the rf dependence of the dispersion mode.

In the particularly favorable instance when $Z\|Z'$, $\theta=0$ and Eq. (32) reduces to the familiar Bloch-like form

$$M_{y'}{}^{\cos}=\frac{8\gamma M_0\Delta\omega T_2{}^3\Omega H_1}{(1+\sigma+\Delta\omega^2T_2{}^2)^2}.$$

VI. EXPERIMENTAL APPARATUS AND METHODS

Our nuclear-induction equipment was a slightly modified Varian wide-line spectrometer (VF-16). The V4210A rf unit was altered to allow a narrow range of frequency scan by means of an external variable capacitor and clock-motor arrangement. ^{14}N resonances in hexamethylenetetramine were observed at about 3.308 MHz using a Varian V4230B 2–4 MHz nuclear induction probe with the V4210A. A sinusoidal magnetic field in the probe sweep coils was generated by a Varian V4250A sweep unit, and static magnetic fields could be supplied, as needed, by a 20.6-cm-diam Helmholtz pair coaxial with the probe sweep coils. The signal from the V4210A was fed to a V4270A phase-sensitive detector and amplifier and then to a Varian G-14 recorder. Auxiliary equipment included a Hewlett-Packard Model 524B counter for measuring the radio frequency, and power supplies, and amplifiers as needed.

The transmitter coil, pickup coil, and field sweep coils of the probe are mutually orthogonal, and thus conform to the X', Y', and Z' axes as defined above.

The samples were polycrystalline hexamethylenetetramine in both the as-received and purified[32] states. Quite large signals could be observed from the loosely packed powder.

In order to minimize stray magnetic field effects, the Z' axis (magnetic field axis) of the probe was aligned in the direction of minimum ambient field. In this direction, the local field was less than 0.03 Oe.

The apparatus, by means of the probe paddles, could be tuned to observe either the absorption (V) or dispersion (U) modes. As seen above, the signals are actually derivatives of these modes. In Fig. 4 recorder tracings of the derivative V and U modes are displayed. It can be seen that an anomalous, and for the present unexplained, signal structure is present.[33] This structure is present for both purified and unpurified samples. For high enough magnetic modulation, the signal-to-noise ratio increases and the anomalous signal structure

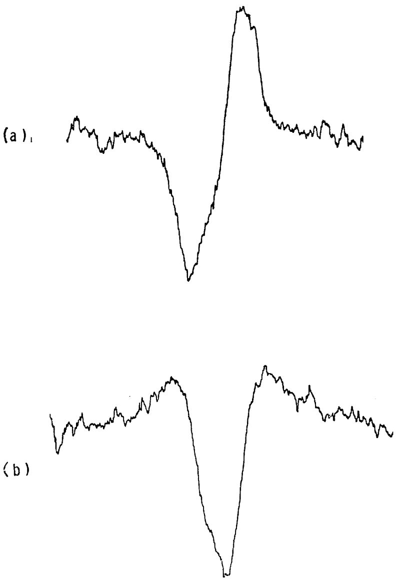

FIG. 4. Experimental NQR induction-absorption (V) and (negative) dispersion (U) mode tracings for polycrystal hexamethylenetetramine. Signals were taken with nondistorting modulation. Note the signal asymmetry discussed in text. Frequency increases from right to left. NQR induction method automatically gives derivative-type signals as explained in text.

---

[32] The author is grateful to Dr. T. J. Mao for purification of the sample.

[33] It has been suggested that the anomaly may be due to spin quenching (see Ref. 15). However, since the main source of line broadening is due to protons, one might expect quenching effects to be small in hexamethylenetetramine for which $\eta=0$.

is smoothed out and disappears. Scott[34] has seen similar structure in solid N_2 in which the anomaly was observable using both frequency modulation and Zeeman modulation. Scott[35] has suggested that the slight asymmetry in the Zeeman modulated signal of hexamethylenetetramine as seen by Watkins and Pound[18] may be evidence for such an anomaly in this substance. Anomalies in solid ND_3 and hexamethylenetetramine have been reported by O'Konski and Flautt.[36] In the present work the anomalous line shape undoubtedly affects the comparison with theory. This is not too disturbing since the present theory has built into it the highly idealized Lorentzian line shape anyway. We shall see that the dependence of many measured quantities (such as linewidth) on experimental parameters (such as modulation amplitude) is relatively insensitive to line shape.

Three experimental aspects were studied. (1) Since the V mode is most frequently the signal of interest, the effect of magnetic modulation field, $h_m \cos\omega_m t$, on V-mode line shape, width, and intensity was determined. These measurements were performed at low rf levels in the absence of a static magnetic field (except for ambient fields). (2) The effect on the V-mode signal of a static magnetic field h_s along Z' was also determined. These studies were made with a fixed low modulation field and low rf level. Again the line shape, width, and intensity were measured. (3) The effect of rf level on both the U- and V-mode signals was determined for a fixed low magnetic modulation and small ambient static fields.

VII. COMPARISON OF THEORY AND EXPERIMENT

In this section emphasis is placed on the theoretical results for polycrystalline samples since suitable single crystals were not available. However, theoretical results for optimally oriented single crystals of equivalent nuclei are presented in tabular form.

A. Modulation Effects

In our study of modulation effects, we follow the notation of Ref. 29 and express the modulation intensity $h_m(=\frac{1}{2}$ the peak-to-peak swing) as a dimensionless quantity by normalizing to the true line width, δH (gauss), between points of slope extrema. In terms of the true line width, $\delta\nu$, in frequency units (as found from experiment using low modulations) the relation needed is $\delta H = 2\pi\delta\nu/\gamma = \delta\omega/\gamma$, and our dimensionless modulation parameter becomes $\gamma h_m/\delta\omega$.

Since the theoretical line is Lorentzian, its true width is given by $T_2\delta\omega = 2/\sqrt{3}$. Consequently, we have, in terms of the theory, $\gamma h_m/\delta\omega = \epsilon_m\sqrt{3}/2 = 0.866\epsilon_m$.

1. Line Shape

Because of the anomalous signal structure mentioned above, determination of the true line shape is difficult. However, the ratio of the inner to the outer slope extrema of the V-mode derivative signal was roughly 2. For a Gaussian line this ratio is 2.2, for a Lorentzian, 4.0.[31]

V-mode experimental tracings for various modulation fields are shown in Fig. 5, where they are compared with theoretical polycrystal signals. The theoretical curves were calculated from Eq. (29) with $\epsilon_s = 0$, using an IBM 7094 computer and a FORTRAN II program. The behavior of the experimental and theoretical curves is qualitatively similar.

2. Linewidth

The theoretical dependence of the calculated measured linewidth, $\delta\omega_{\text{meas}} = 2\pi\delta\nu_{\text{meas}} = \gamma\delta H_{\text{meas}}$, on modulation amplitude was found by solving Eq. (30) numerically on an IBM 7094. For convenience in comparing theory and experiment, the scheme of Ref. 29 was followed, in that the measured line width was normalized to the true line width, $\delta\omega$. The experimental true line width at room temperature $\delta\nu = 0.526$ kHz, corresponds to $\delta H = \delta\omega/\gamma = 1.71$ G. Matzkanin *et al.*[37]

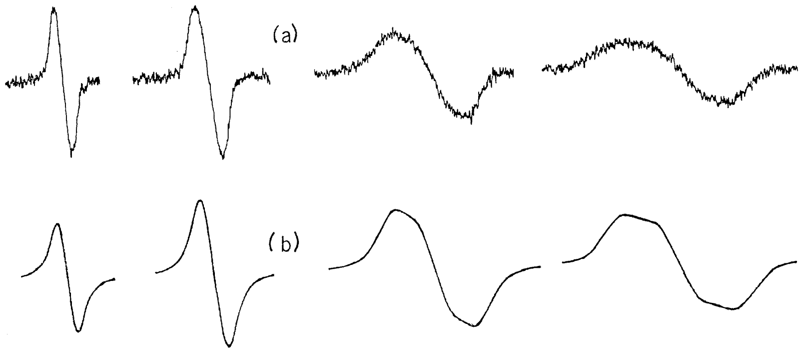

FIG. 5. Effect of modulation amplitude on polycrystal NQR-induction V-mode line shapes. (a) Experiment. (b) Theory. From left to right the modulation parameter $\gamma h_m/\delta\omega$ is about 0.72, 1.4, 4.4, and 6.2 for both. The amplitude discrepancy is a line-shape effect discussed in the text. Note that for wide lines the frequency scan is nonlinear.

---

[34] T. A. Scott, J. Chem. Phys. **36**, 1459 (1962).
[35] T. A. Scott (private communication).
[36] C. T. O'Konski and T. J. Flautt, J. Chem. Phys. **27**, 815 (1957).
[37] G. A. Matzkanin, T. N. O'Neal, T. A. Scott, and P. J. Haigh, J. Chem. Phys. **44**, 4171 (1966).

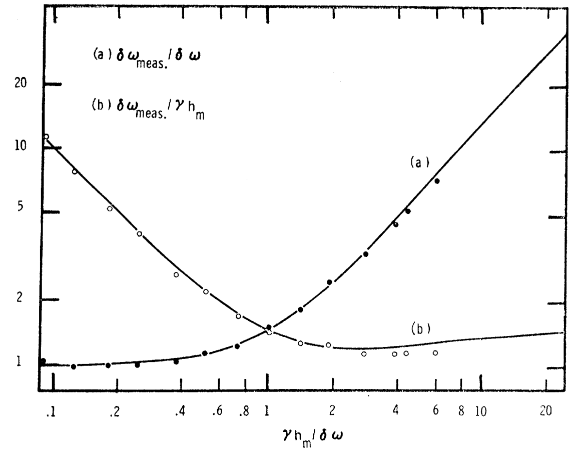

FIG. 6. Effect of modulation amplitude on polycrystal NQR-induction V-mode linewidth. (a) $\delta\omega_{meas}/\delta\omega$ versus $\gamma h_m/\delta\omega$. (b) $\delta\omega_{meas}/\gamma h_m$ versus $\gamma h_m/\delta\omega$. Points are experimental results; solid curves are theory.

TABLE. I. Calculated effect of modulation amplitude on NQR induction signal (no saturation, no static field).[a]

	Single Crystal ($\theta=0$)			Polycrystal		
$\frac{\gamma h_m}{\delta\omega}$	$\frac{\delta\omega_{meas}}{\delta\omega}$	$\frac{\delta\omega_{meas}}{\gamma h_m}$	$\frac{(a_1)_{max}}{C}$	$\frac{\delta\omega_{meas}}{\delta\omega}$	$\frac{\delta\omega_{meas}}{\gamma h_m}$	$\frac{(a_1)_{max}}{0.41C}$
0	1.000	∞	0	1.000	∞	0
0.0866	1.006	11.6	0.129	1.005	11.6	0.105
0.1732	1.032	5.96	0.253	1.018	5.88	0.208
0.2598	1.067	4.11	0.369	1.041	4.01	0.306
0.3464	1.119	3.23	0.475	1.070	3.09	0.399
0.4330	1.179	2.72	0.569	1.107	2.56	0.486
0.5196	1.254	2.41	0.651	1.150	2.21	0.565
0.6928	1.436	2.07	0.779	1.256	1.81	0.699
0.8660	1.645	1.90	0.867	1.380	1.59	0.802
1.299	2.29	1.76	0.973	1.749	1.35	0.952
1.732	3.00	1.73	0.999	2.17	1.25	0.998
1.819	3.15	1.73	1.000	2.27	1.25	1.000
1.905	3.31	1.73	0.9997	2.35	1.24	1.000
1.992	3.45	1.73	0.999	2.44	1.23	0.998
2.078	3.60	1.73	0.997	2.55	1.23	0.996
2.165	3.74	1.73	0.995	2.63	1.22	0.992
2.252	3.90	1.73	0.992	2.74	1.22	0.987
2.338	4.05	1.73	0.989	2.84	1.22	0.981
2.598	4.49	1.73	0.977	3.15	1.21	0.960
3.464	5.95	1.72	0.931	4.26	1.23	0.874
5.196	8.68	1.67	0.837	6.67	1.28	0.716
8.660	14.12	1.63	0.735	11.8	1.36	0.519
17.32	28.06	1.62	0.670	24.6	1.42	0.309
34.64	56.12	1.62	0.650	51.4	1.49	0.173

[a] Note that at low $\gamma h_m/\delta\omega$, (a_1)max for polycrystal $=\frac{1}{3}(a_1)$max for single crystal. Above amplitudes are normalized to 1.000.

find $\delta\nu=0.690$ kHz from 4.2 to 299°K. The source of the discrepancy between our result and theirs is not clear. It is difficult to ascribe the difference to spin quenching since for hexamethylenetetramine ($\eta=0$) the dominant line broading mechanism is taken to be H-N coupling, which should not be quenched for $\eta=0$. A possible source of the larger value of $\delta\nu$ given by Ref. 37 would be over modulation or saturation broadening or perhaps broadening due to ambient magnetic fields, which can be sizable, as we shall see.

In Fig. 6(a) are plotted the theoretical and experimental results for $\delta\omega_{meas}/\delta\omega$ as a function of the modulation parameter $\gamma h_m/\delta\omega$. The behavior is reminiscent of that for magnetic resonance,[29] but differs from it quantitatively. Theory and experiment agree fairly well.

Another way of examining the same data is by plotting the theoretical and experimental values of $\delta\omega_{meas}/(\gamma h_m)$. We see in Fig. 6(b), that as $h_m\rightarrow\infty$, this ratio approaches 2.0 much more slowly than for magnetic resonance.[29]

Table I lists the theoretical values of $\delta\omega_{meas}/\delta\omega$ and $\delta\omega_{meas}/(\gamma h_m)$ as functions of $\gamma h_m/\delta\omega$ for both single crystal and polycrystal samples.

3. *Signal Amplitude*

In Fig. 7 the theoretical dependence of the normalized polycrystal signal amplitude on modulation amplitude is given by the solid curve. The experimental points

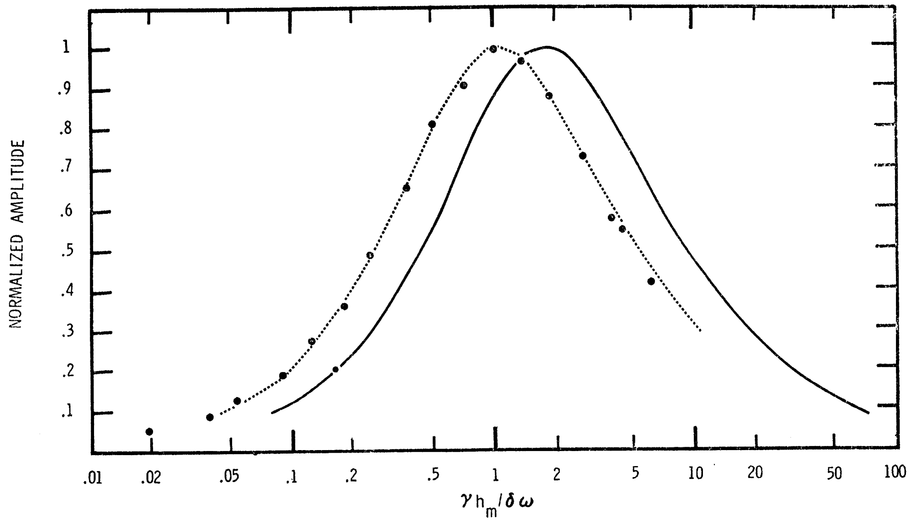

FIG. 7. Effect of modulation on observed polycrystal NQR-induction V-mode signal amplitude. Points are data; solid curve is theory (with built-in Lorentzian signal shape); dashed curve is theory shifted to low h_m by a factor 0.58 to compensate for the fact that signal shape is roughly Gaussian (see text). *Note added in proof.* The point on the solid curve is erroneous and should be deleted.

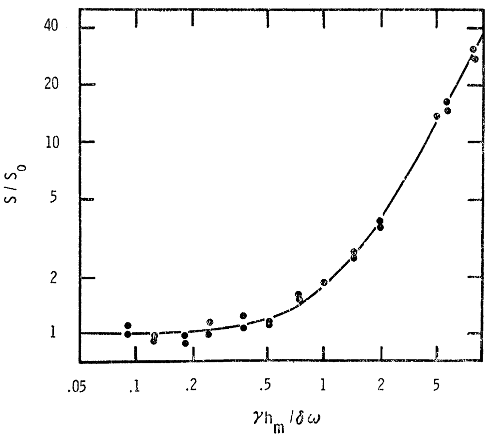

FIG. 8. Effect of modulation on polycrystal NQR-induction V-mode second moment. Points are data; solid curve represents Eq. (39).

are shifted somewhat to low amplitudes with respect to the theory. However, this is not surprising since we know[29] that in magnetic resonance the modulation-dependent amplitude curve for a Gaussian line is shifted by a factor 0.54 to lower h_m than the curve for a Lorentzian. The dashed curve of Fig. 7 is the theoretical curve shifted to low h_m by a factor 0.58. The shift of the amplitude curve is consistent with the fact that the line shape is closer to Gaussian than Lorentzian. We do not necessarily expect the line-shape shift in the cases of magnetic resonance and NQR induction to be the same because of the angle dependence of the magnetic modulation term for NQR. It appears that, as for magnetic resonance,[29] the field dependence of the NQR induction signal amplitude is a more sensitive function of signal shape than is the field dependence of the linewidth.

The theoretical dependence of amplitude on modulation for single and polycrystals is given in Table I. The amplitude has a maximum as a function of h_m because low fields are necessary to produce any signal at all, but large fields broaden and flatten the signal.

4. *Second Moment*

The experimental second moments S for powdered hexamethylenetetramine were determined by numerical integration of line tracings using an IBM 7094 computer program based on a method of Janzen.[38] At low modulations the undistorted room-temperature second moment, S_0, is 0.0765 kHz^2 or 0.81 G^2. (Matzkanin *et al.*[37] find S to be about 25% larger at 77°K.) As the modulation amplitude is increased, the line is broadened, and S increases in a manner qualitatively reminiscent of magnetic resonance.[30] In Fig. 8 the points show the dependence of the experimental second moment (as normalized to S_0) upon the modulation parameter.

Because of the angle dependence of magnetic field effects, it is perhaps not surprising that the increase in S (in G^2) is not given by the Andrew[30] term $h_m^2/4$. The averaging over angle reduces the effectiveness of the magnetic modulation so that instead, a good empirical fit to the data is now given by

$$S=S_0+0.207h_m^2 \quad (\text{in G}^2).$$

An alternative form of the same expression is, for the hexamethylenetetramine data,

$$S=S_0\left[1+\frac{3}{4}\left(\frac{\gamma h_m}{\delta\omega}\right)^2\right]. \qquad (39)$$

Equation (39) is plotted in Fig. 8 as a solid curve. The fit to the data is satisfactory.

B. Static Field Effects

In these experiments the modulation amplitude, h_m, was kept at a low, nondistorting level, while the static field strength h_s was changed, step-wise from one experimental run to another. As mentioned above, the probe was so placed that the ambient field parallel to h_s was zero. Values of h_s were both calculated from the Helmholtz coil equation and checked experimentally using a Hall effect probe. The static field, in the following discussions, is expressed as a dimensionless parameter, $\gamma h_s/\delta\omega$ (or $0.866\epsilon_s$ for the theoretical Lorentzian line).

1. *Line Shape*

Experimental and theoretical polycrystal V-mode tracings are shown in Fig. 9 for various strengths of h_s. The theoretical curves are plots of Eq. (29) for ϵ_m small and various ϵ_s values. Computations were made on an IBM 7094.

Theory and experiment agree in the qualitative behavior of the polycrystal line shape. Both show the appearance of line splitting at relatively small values of h_s. Furthermore, experiment and theory agree that a sufficient increase of h_m will smear out the splitting so that only a broadened line is observed. This is consistent with Fig. 5 which shows that splitting does not appear for fairly large h_m, although some structure does appear.

In essence, the structure of the signal for large h_s can be regarded as being due to the superposition of two derivative signals, equally displaced about the central frequency.

2. *Linewidth*

The theoretical dependence of the measured polycrystalline linewidth, $\delta\omega_{\text{meas}}$, on static field amplitude was found by solving Eq. (30) numerically, as previously mentioned. For values of h_s large enough to produce splitting, $\delta\omega_{\text{meas}}$ is the separation of the outermost extrema.

In Fig. 10(a) are plotted the polycrystalline theoreti-

---

[38] G. W. Smith, J. Chem. Phys. 42, 4229 (1965); 43, 4325 (1965).

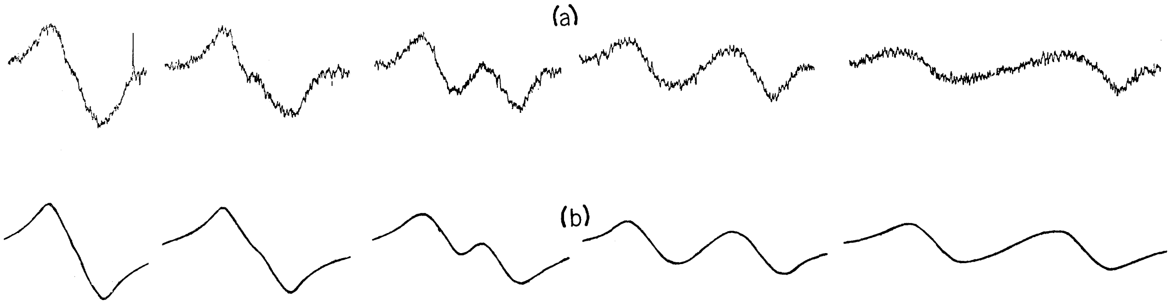

FIG. 9. Effect of static magnetic field on polycrystal NQR-induction *V*-mode line shape. (a) Experiment for $\gamma h_s/\delta\omega = 0.396$, 0.544, 0.873, 1.59, and 2.44, respectively. (b) Theory for $\gamma h_s/\delta\omega = 0.433$, 0.566, 0.892, 1.65, and 2.41, respectively. Experimental modulation parameter $\gamma h_m/\delta\omega = 0.37$; in theory modulation parameter taken as 0.19 (in either case, modulation is effectively nondistorting). Note that experimental frequency scan is nonlinear. In first trace, total scan is about 1.7 kHz.

cal and experimental results for $\delta\omega_{\text{meas}}/\delta\omega$ as a function of the static field parameter $\gamma h_s/\delta\omega$. The behavior is somewhat like that of Fig. 6(a), but it is apparent that the measured linewidth is more sensitive to static field than modulation field. The agreement of theory and experiment is good.

A plot of theoretical and experimental $\delta\omega_{\text{meas}}/(\gamma h_s)$ is shown in Fig. 10(b). We see that $\delta\omega_{\text{meas}}$ approaches $2\gamma h_s$ fairly rapidly. However, in contrast to the behavior for both NQR induction and magnetic resonance with h_m, $\delta\omega_{\text{meas}}/(\gamma h_s)$ is monotonically decreasing.

Table II lists the theoretical values of $\delta\omega_{\text{meas}}/\delta\omega$ and $\delta\omega_{\text{meas}}/(\gamma h_s)$ as functions of $\gamma h_s/\delta\omega$ for both single and polycrystals.

3. *Signal Amplitude*

In Fig. 11 the theoretical dependence of polycrystal signal amplitude at outer extrema on h_s is plotted as a solid curve. The experimental data, as normalized to the zero field value, are shifted to low h_s with respect to the theory. This shift, like that for amplitude as a function of h_m, is probably at least partly due to the non-Lorentzian line shape. Some of the deviation may be due to the extreme sensitivity of the signal to static fields (which may include stray ambient fields).

Table II gives the dependence of single and polycrystal signal amplitude upon static field strength.

The fact that the amplitude is a monotonically decreasing function of h_s is due to the nature of the phase-sensitive method. The modulating field h_m serves simultaneously to remove energy-level degeneracy and to act as a reference signal for the phase-sensitive detector. The static field h_s contributes essentially nothing to the component of the signal at the modulation frequency, but it does produce broadening and hence diminishes the signal intensity.

FIG. 10. Effect of static magnetic field on polycrystal NQR induction *V*-mode linewidth; points are data; solid curves are theory. (a) $\delta\omega_{\text{meas}}/\delta\omega$ versus $\gamma h_s/\delta\omega$. (b) $\delta\omega_{\text{meas}}/\gamma h_s$ versus $\gamma h_s/\delta\omega$.

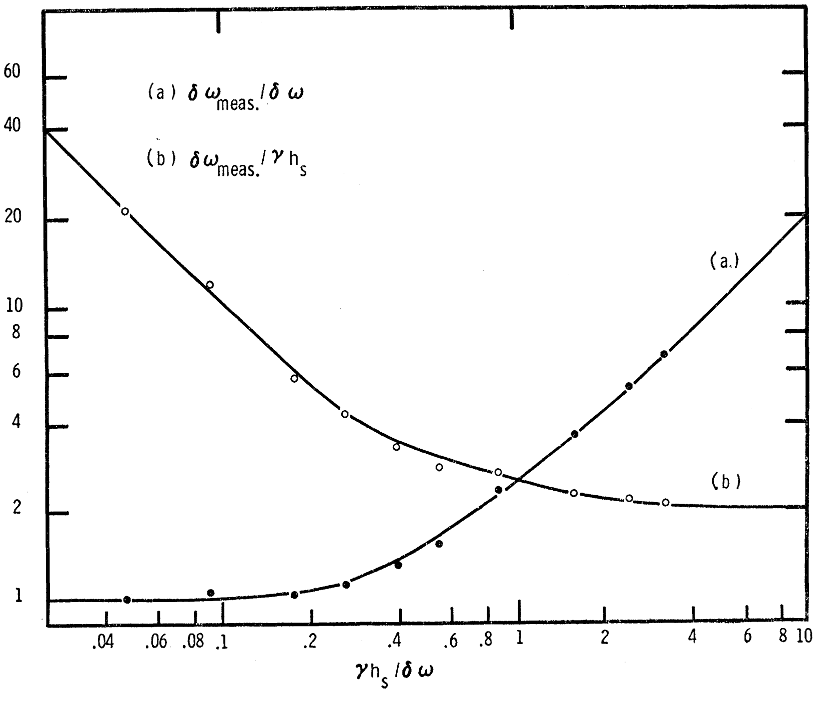

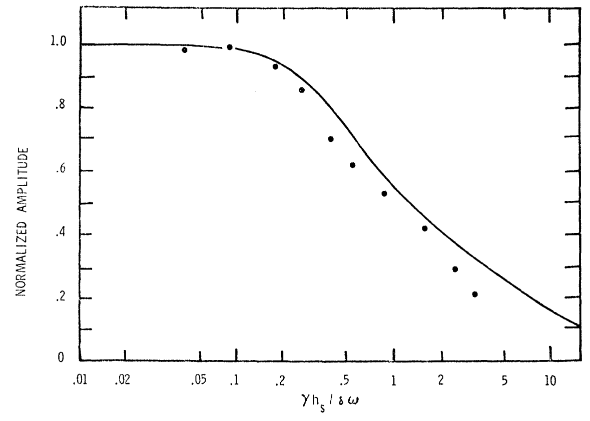

FIG. 11. Effect of static magnetic field on observed polycrystal NQR-induction V-mode signal amplitude. Points are data; solid curve is theory. Experimental and theoretical amplitudes $=1.00$ at $\gamma h_s/\delta\omega=0$.

However, calculations show that in an experiment using a sensitive, broad-band detector and a static field only, the amplitude would show a maximum as a function of h_s. In essence, these calculations are merely solutions of Eq. (21). In this "static field only" experiment the field is needed to remove the degeneracy, but it also acts to broaden the line. As mentioned earlier, noise considerations make this technique unusable.

4. *Second Moment*

In Fig. 12 is shown the experimental dependence of the polycrystal second moment upon the static field parameter. The second moments were determined as in Sec. VII. A.4. We see that S increases with h_s in spite of the negative portions of the signal which appear at large h_s values (Fig. 9). This increase of S is not surprising since large fields, in addition to producing a complex line structure, broaden the line and shift portions considerably. Because of these complexities, we find that no simple correlation of S with h_s^2 exists. The solid curve of Fig. 12 is merely a hand-drawn fit to the data.

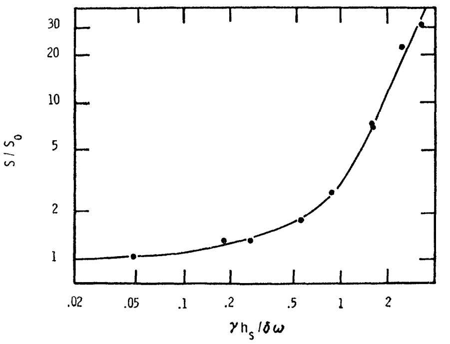

FIG. 12. Effect of static magnetic field on experimental polycrystal NQR-induction V-mode second moment. Points are data; solid curve is smooth fit to data. Second moments were determined from curves like those of Fig. 9(a).

C. Saturation Effects

Since Eqs. (36) and (38) contain factors of H_1, let us follow the usual practice[31] and remove this portion of the rf dependence by dividing it out. Furthermore, we wish to normalize the resulting expressions to 1 at $\sigma=0$. The normalized equations are

$$V_{\max}/H_1=\frac{1}{(1+\sigma)^{3/2}}\left[1+0.3\left(\frac{\sigma}{1+\sigma}\right)+0.145\left(\frac{\sigma}{1+\sigma}\right)^2+0.080\left(\frac{\sigma}{1+\sigma}\right)^3+0.047\left(\frac{\sigma}{1+\sigma}\right)^4+\cdots\right], \quad (36a)$$

$$U_{\max}/H_1=\frac{1}{1+\sigma}\left[1+0.2\left(\frac{\sigma}{1+\sigma}\right)+0.0857\left(\frac{\sigma}{1+\sigma}\right)^2+0.0476\left(\frac{\sigma}{1+\sigma}\right)^3+0.0303\left(\frac{\sigma}{1+\sigma}\right)^4+\cdots\right]. \quad (38a)$$

Plots of these equations are the saturation curves. In order to fit theory to experiment it is necessary to shift[31] the equations by normalizing σ to the square of the rf voltage, ϵ_{rf}, since H_1 is proportional to ϵ_{rf}. As BPP point out, shifting the saturation curve corresponds to normalizing to $H_1{}^2T_1T_2$. An independent measurement of T_1 plus knowledge of T_2, allows one to determine relative changes in T_1 from the saturation-curve method. In the following sections the data were taken at 300°K.

1. *V-Mode Saturation Curve*

In Fig. 13 are plotted experimental $V_{\max}/H_1$ data points as a function of ϵ_{rf}. Equation (36a), as nor-

TABLE II. Calculated effect of static field on NQR induction signal (no saturation, no modulation broadening).

	Single Crystal ($\theta=0$)			Polycrystal		
$\frac{\gamma h_s}{\delta\omega}$	$\frac{\delta\omega_{\text{meas}}}{\delta\omega}$	$\frac{\delta\omega_{\text{meas}}}{\gamma h_s}$	Norm Amp	$\frac{\delta\omega_{\text{meas}}}{\delta\omega}$	$\frac{\delta\omega_{\text{meas}}}{\gamma h_s}$	3× (Norm. Amp.)
0	1.000	∞	1.000	1.000	∞	1.000
0.0433	1.015	23.44	0.994	1.007	23.26	0.996
0.0866	1.036	11.96	0.978	1.018	11.76	0.985
0.1732	1.129	6.52	0.921	1.077	6.22	0.948
0.2165	1.199	5.54	0.884	1.115	5.15	0.925
0.2598	1.285	4.95	0.846	1.169	4.50	0.896
0.3464	1.481	4.27	0.773	1.295	3.74	0.835
0.4330	1.697	3.92	0.712	1.446	3.34	0.776
0.5196	1.905	3.67	0.666	1.597	3.07	0.723
0.6928	2.312	3.34	0.605	1.960	2.83	0.639
0.8660	2.685	3.10	0.569	2.300	2.65	0.580
1.299	3.585	2.76	0.529	3.118	2.40	0.490
1.516	4.018	2.65	0.520	3.53	2.33	0.461
1.732	4.460	2.58	0.515	3.93	2.27	0.437
2.598	6.201	2.39	0.505	5.58	2.15	0.367
3.464	7.933	2.29	0.502	7.24	2.090	0.318
5.196	11.40	2.19	0.501	10.61	2.044	0.251
6.928	14.86	2.15	0.500	14.03	2.025	0.206
8.660	18.32	2.12	0.500	17.47	2.018	0.175
17.32	35.65	2.06	0.500	34.7	2.005	0.0998
34.64	70.32	2.03	0.500	69.3	2.001	0.0535
69.28	139.6	2.02	0.500	138.6	2.000	0.0277

malized, is plotted as a solid curve. In spite of the experimental scatter, the agreement is satisfactory.

2. *U-Mode Saturation Curve*

Figure 14 shows data and theory for the $U_{\max}/H_1$ as a function of ϵ_{rf}. The solid curve is Eq. (38a) normalized using the normalization factor for σ determined for the V-mode curve of Fig. 13. This factor is obviously not correct for the U mode, and a suitably shifted theoretical plot is shown as a dashed curve. This discrepancy between the U- and V-mode normalization factors may be due in part to three causes: (1) the necessity of approximating the position of the V-mode signal extrema (see Sec. V.A); (2) the non-Lorentzian line shape; and (3) the neglect of passage effects (our experiment may be closer to case II of BPP than to case I). The approximation in the first case corresponds to the assumption that the linewidth is proportional to $(1+\sigma)^{-1/2}$. An experimental check of this assumption showed that it is indeed correct, but that the normalization constant between σ and ϵ_{rf}^2 is different from those of the U- and V-mode saturation curves.

In Table III, Eqs. (36a) and (38a) are evaluated as a function of σ. Also tabulated are the values of the BPP case I V- and U-mode functions, $(1+\sigma)^{-3/2}$ and $(1+\sigma)^{-1}$, which are the leading terms in Eqs. (36a) and (38a). It appears that the difference between the BPP case and Eqs. (36a) and (38a) does not become appreciable (~10%) until $\sigma \cong 0.5$.

TABLE III. Calculated effect of rf for polycrystal (no static field, no modulation broadening).

σ	$(1+\sigma)^{-3/2}$	$V_{\max}/H_1$	$(1+\sigma)^{-1}$	$U_{\max}/H_1$
10^{-3}	0.999	0.999	0.999	0.999
10^{-2}	0.985	0.988	0.990	0.992
2×10^{-2}	0.971	0.976	0.980	0.984
4×10^{-2}	0.943	0.954	0.962	0.969
6×10^{-2}	0.916	0.932	0.943	0.954
8×10^{-2}	0.891	0.911	0.926	0.940
0.1	0.867	0.892	0.909	0.926
0.2	0.761	0.802	0.833	0.863
0.3	0.675	0.727	0.769	0.809
0.4	0.604	0.664	0.714	0.761
0.5	0.544	0.609	0.667	0.719
0.6	0.494	0.562	0.625	0.681
0.7	0.451	0.521	0.588	0.648
0.8	0.414	0.485	0.556	0.617
1.0	0.354	0.424	0.500	0.565
1.2	0.306	0.375	0.454	0.520
1.4	0.269	0.335	0.417	0.483
1.6	0.239	0.302	0.385	0.450
1.8	0.213	0.274	0.357	0.422
2.0	0.192	0.250	0.333	0.397
3.0	0.125	0.169	0.250	0.307
4.0	0.089	0.125	0.200	0.250
5.0	0.068	0.097	0.167	0.211
6.0	0.054	0.078	0.143	0.183
8.0	0.037	0.054	0.111	0.144
9.0	0.032	0.047	0.100	0.130
10.0	0.027	0.041	0.091	0.119

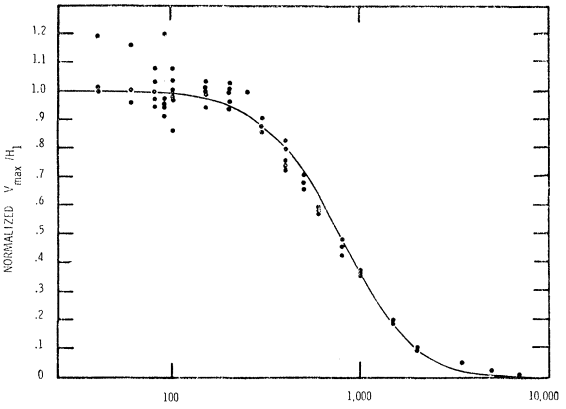

FIG. 13. Effect of saturation on maximum recorder swing of observed polycrystal V-mode signal. Solid curve is fit of Eq. (36a) to data.

VIII. THE THEORY APPLIED TO SINGLE-COIL (ABSORPTION) EXPERIMENTS

A. Preliminary Considerations

Although the present theory was evolved to explain the NQR induction method, it is apparent that it is easily applicable to single-coil or absorption-type experiments. We shall consider three possible experimental methods: sinusoidal magnetic modulation, Zeeman (square-wave magnetic) modulation, and frequency modulation. The latter two methods are the usual NQR single-coil modulation techniques.

The quantity to be calculated, instead of $M_{y'}$ Eq. (7), is $M_{x'}$, the magnetization along the transmitter coil itself:

$$M_{x'} = M_x^{\mathrm{total}} \cos(X,X') + M_y^{\mathrm{total}} \cos(Y,X'). \tag{40}$$

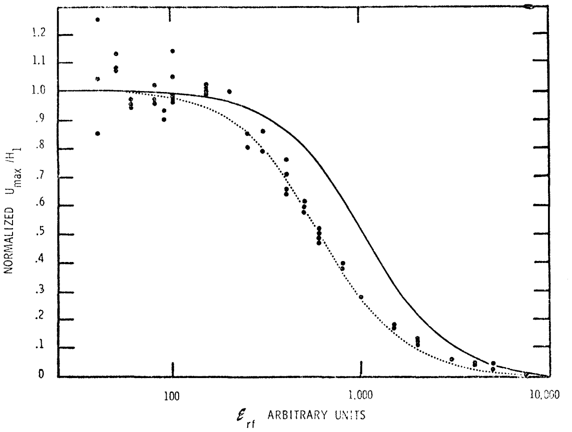

FIG. 14. Effect of saturation on maximum recorder swing of observed polycrystal U-mode signal. Solid curve is Eq. (38a) using normalization constant for σ as obtained from fit of Fig. 13. Dashed curve is a fit of theory to U-mode data.

In terms of the Euler angles we have[26]

$$\cos(X,X')=\hat{\imath}\cdot\hat{l}=\cos\varphi\cos\psi-\sin\varphi\sin\psi\cos\theta$$

$$\cos(Y,X')=\hat{\jmath}\cdot\hat{l}=\sin\varphi\cos\psi+\cos\varphi\sin\psi\cos\theta.$$

The calculations proceed similarly to those for the induction signal, except that now the $\cos\omega t$ term yields the dispersion mode and the $\sin\omega t$ term the absorption mode.

1. *Dispersion Mode* (*cosωt Term*)

The exact solution is

$$M_{x'}{}^{\cos}=\frac{2C\Delta\omega T_2(1-\sin^2\psi\sin^2\theta)[s+(\Delta\omega^2-\Omega^2\cos^2\theta)T_2{}^2]}{[s+(\Delta\omega+\Omega\cos\theta)^2T_2{}^2][s+(\Delta\omega-\Omega\cos\theta)^2T_2{}^2]}. \tag{41}$$

For no saturation ($s=1$) and low fields ($\Omega\approx 0$),

$$M_{x'}{}^{\cos}=\frac{2C\Delta\omega T_2(1-\sin^2\psi\sin^2\theta)}{1+\Delta\omega^2T_2{}^2}, \tag{42}$$

which is indeed a dispersion-like signal.

2. *Absorption Mode* (*sinωt Term*)

The magnetization is

$$M_{x'}{}^{\sin}=\frac{2C[s+(\Delta\omega^2+\Omega^2\cos^2\theta)T_2{}^2](1-\sin^2\psi\sin^2\theta)}{[s+(\Delta\omega+\Omega\cos\theta)^2T_2{}^2][s+(\Delta\omega-\Omega\cos\theta)^2T_2{}^2]}, \tag{43}$$

which for $s=1$, $\Omega\approx 0$ becomes

$$M_{x'}{}^{\sin}=\frac{2C(1-\sin^2\psi\sin^2\theta)}{1+\Delta\omega^2T_2{}^2}, \tag{44}$$

a Lorentzian absorption signal.

B. Sinusoidal Magnetic Modulation, Phase-Sensitive Detection, Absorption Signal

Let us now derive the absorption signal for a single crystallite, in the absence of saturation ($s=1$). Letting $\beta=\Delta\omega T_2$ and $\epsilon_\theta=\Omega T_2\cos\theta$, we have from Eq. (43)

$$M_{x'}=\frac{2C(1+\beta^2+\epsilon_\theta{}^2)(1-\sin^2\psi\sin^2\theta)}{[1+(\beta+\epsilon_\theta)^2][1+(\beta-\epsilon_\theta)^2]}. \tag{45}$$

With sinusoidal modulation, ϵ_θ becomes $\epsilon_m\cos\omega_m t=\epsilon_m\cos\theta_m$, where ϵ_m is understood to be a function of θ. The equation for the signal [coefficient a_1 in Eq. (28)] becomes

$$a_1=\frac{4C(1-\sin^2\psi\sin^2\theta)}{\pi}\int_0^\pi\frac{(1+\beta^2+\epsilon_m{}^2\cos^2\theta_m)\cos\theta_m d\theta_m}{[1+(\beta+\epsilon_m\cos\theta_m)^2][1+(\beta-\epsilon_m\cos\theta_m)^2]}\equiv 0. \tag{46}$$

Equation (46) is identically zero because $\cos\theta_m$ is antisymmetric about $\pi/2$, and the remainder of the integrand is symmetric about $\pi/2$. Hence, no absorption signal is seen. The dispersion signal is also predicted to be identically zero. Since the signal for any crystallite is zero, the signal of a polycrystalline sample is zero.

This result was substantiated experimentally. B. W. Joseph, of our laboratory, performed a sinusoidal magnetic modulation, phase-sensitive detection, single-coil experiment using an externally quenched superregenerator.[39] The instrument was adjusted so that a ^{35}Cl resonance in *p*-dichlorobenzene was easily observable on an oscilloscope when frequency modulation methods were used. However, in the sinusoidal magnetic-modulation experiment no appreciable signal was recorded. Although ^{35}Cl has $I=\frac{3}{2}$ (and $\eta=0.08$ in *p*-dichlorobenzene[40]), the above arguments are still expected to be qualitatively correct, as we shall see below when we discuss the extension of the present theory to higher spins.

It is probable that phase-sensitive detection at harmonics of the modulation frequency will produce useful signals for sinusoidal magnetic modulation.

C. Zeeman Modulation, Phase-Sensitive Detection, Absorption Signal

Zeeman (magnetic-square-wave) modulation is frequently used with phase-sensitive detection techniques to observe NQR resonances. Negita[13] has given a rather complete quantum-mechanical consideration of Zeeman-modulated Lorentzian and Gaussian NQR

---

[39] J. M. Velten and H. S. Story, Am. J. Phys. **33**, 32 (1965).

[40] H. C. Meal, J. Am. Chem. Soc. **74**, 6121 (1952); quoted in Ref. 6, p. 159.

lines. Therefore, we shall only briefly discuss the present treatment with its Lorentzian shape. By slightly modifying the approach of Sec. VIII.B, we can derive a theoretical expression for the absorption signal. The arguments which follow are equally applicable either for off-on magnetic modulation between 0 and h_z (with phase-sensitive detection at the modulation frequency[18]) or for antisymmetric Zeeman modulation (with detection at twice the modulation frequency[41]). The modulation parameter is $\epsilon_z=\gamma h_z T_2$, and all other parameters retain their previous meanings.

1. *Single Crystal, No Saturation*

Equation (45) is applicable to this situation, but ϵ_θ is now a square wave alternating between 0 and $\epsilon_z\cos\theta$. With phase-sensitive detection at the modulation frequency, ω_m, our integration of the expression for signal amplitude

$$a_1=\frac{1}{\pi}\int_{-\pi}^{\pi} M_{x'}\cos\theta_m d\theta_m,$$

where $\theta_m=\omega_m t$, can no longer be reduced to an integral from 0 to π for symmetry reasons. We have

$$\begin{aligned}a_1&=\frac{2C(1-\sin^2\psi\sin^2\theta)}{\pi}\int_{-\pi}^{\pi}\frac{(1+\beta^2+\epsilon_\theta^2)\cos\theta_m d\theta_m}{[1+(\beta+\epsilon_\theta)^2][1+(\beta-\epsilon_\theta)^2]}\\&=\frac{4C(1-\sin^2\psi\sin^2\theta)}{\pi}\\&\quad\times\left\{\frac{1}{1+\beta^2}-\frac{(1+\beta^2+\epsilon_z^2\cos^2\theta)}{[1+(\beta+\epsilon_z\cos\theta)^2][1+(\beta-\epsilon_z\cos\theta)^2]}\right\}\\&=\frac{4C\epsilon_z^2(\cos^2\theta)(1-\sin^2\psi\sin^2\theta)}{\pi(1+\beta^2)}\\&\quad\times\left\{\frac{\epsilon_z^2\cos^2\theta+1-3\beta^2}{[1+(\beta+\epsilon_z\cos\theta)^2][1+(\beta-\epsilon_z\cos\theta)^2]}\right\}.\end{aligned}\tag{47}$$

Equation (47) is an even function of both β and ϵ_z, as it should be for the proper symmetry of the line shape and the proper independence of sign of the Zeeman modulation. The expression for a given ϵ_z has its maximum at $\beta=0$. This maximum a_1 increases monotonically with $\epsilon_z(h_z)$. The dependence of $(a_1)_{\max}$ on Zeeman modulation is illustrated for an optimally oriented single crystal ($\theta=0$) in Fig. 15. The most rapid increase in signal strength occurs when the Zeeman modulation is about equal to the true linewidth (in magnetic field units).

From Eq. (47) we see that a_1 goes to zero at $3\beta^2=(1+\epsilon_z^2\cos^2\theta)$. This corresponds to a measured linewidth at zero amplitude given by

$$\delta\omega_{\text{meas}}{}^0=(\delta\omega^2+\tfrac{4}{3}\gamma^2h_z^2\cos^2\theta)^{1/2}.$$

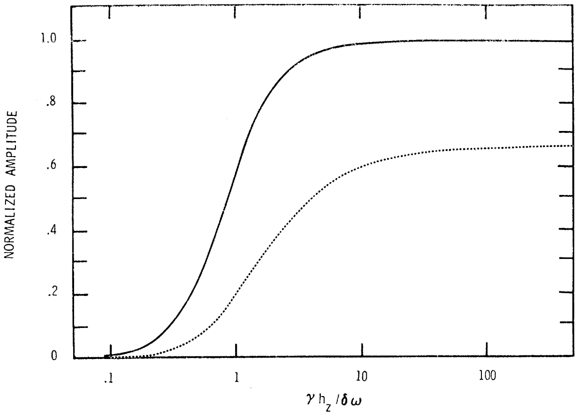

FIG. 15. Theoretical single-crystal and polycrystal amplitudes for Zeeman modulated signals as a function of modulation amplitude. Single-crystal orientation for maximum signal. Single-crystal curve is solid, polycrystal curve dashed.

For large h_z, $\delta\omega_{\text{meas}}{}^0\approx 2\gamma h_z\cos\theta/\sqrt{3}$. The theoretical linewidth behavior is given for $\theta=0$ in Fig. 16.

For $3\beta^2>1+\epsilon_z^2\cos^2\theta$, a_1 is negative, corresponding to the negative wings of a Zeeman modulated signal.

2. *Polycrystal, No Saturation*

The polycrystal signal can be calculated exactly by straightforward averaging of Eq. (47) over θ and ψ. We have

$$\begin{aligned}\bar{a}_1&=\frac{1}{4\pi}\int_0^{\pi}\int_0^{2\pi} a_1\sin\theta d\psi d\theta\\&=\frac{C}{\pi}\left\{\frac{8}{3(1+\beta)^2}-\frac{2}{\epsilon_z^2}+\frac{\beta}{\epsilon_z^3}\ln\frac{1+(\beta+\epsilon_z)^2}{1+(\beta-\epsilon_z)^2}\right.\\&\quad\left.-\frac{(\beta^2+\epsilon_z^2-1)}{\epsilon_z^3}[\tan^{-1}(\beta+\epsilon_z)-\tan^{-1}(\beta-\epsilon_z)]\right\}.\end{aligned}\tag{48}$$

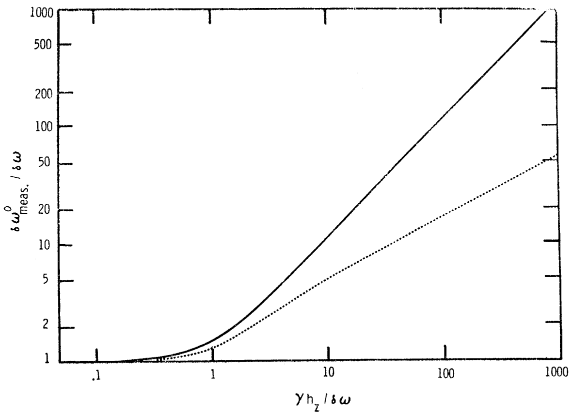

FIG. 16. Effect of Zeeman modulation amplitude on linewidth at zero amplitude for single-crystal and polycrystal. Single-crystal orientation optimized. Single-crystal curve is solid, polycrystal curve dashed.

---

[41] T. A. Scott, Ph.D. thesis, Harvard University, 1959 (unpublished).

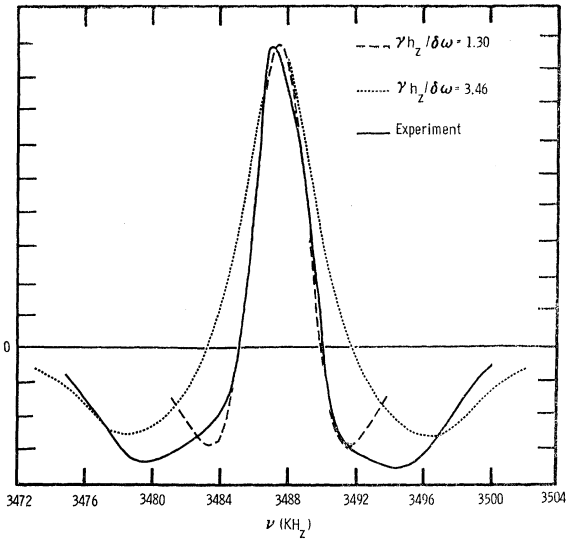

FIG. 17. Comparison of experimental and theoretical Zeeman modulated absorption line shapes for $Z=1$, $\eta=0$ (polycrystalline sample). The experimental curve, shown by the solid line is from Ref. 41. Theoretical curves for $\gamma h_z/\delta\omega=1.30$ and 3.46 are shown by the dashed and dotted lines, respectively.

As required, this expression is even in β and ϵ_z. The line shape given by Eq. (48) shows the proper frequency dependence for a Zeeman modulated line: a maximum at the resonance frequency flanked by netative wings. Equation (48) is equivalent to Eq. (19) of Negita.[13]

The maximum powder signal as a function of Zeeman modulation is shown in Fig. 15. We see that the behavior is qualitatively like that of a single crystal. As expected,[42] the maximum is $\frac{2}{3}$ that for an optimally oriented single crystal.

In Fig. 17 are compared experimental and theoretical Zeeman modulated line shapes. The experimental line is a resonance in solid polycrystalline N_2 with a Zeeman modulation of about 35–37 G.[35,41] Two theoretical polycrystal lines are shown. One, with $\gamma h_z/\delta\omega=3.5$, corresponds to the actual experimental situation.[41] The other, with $\gamma h_z/\delta\omega=1.3$, was chosen to give agreement with the experimental linewidth at zero amplitude. It can be seen that neither theoretical line gives better than qualitative agreement with experiment. The experimental width in Fig. 17 is about 4.8 kHz, and the present theory for $\gamma h_z/\delta\omega=3.5$ gives 8.6 kHz. The discrepancy between experiment and the present theory is presumably due to the fact that the true experimental line shape for solid N_2 is roughly Gaussian.[41] The Gaussian shape has been shown by Negita[13] to give better agreement with experiment. The polycrystal linewidth at zero signal amplitude as given by the zeros of Eq. (48) is plotted in Fig. 16 as a function of $\gamma h_z/\delta\omega$.

Although the present theory of Zeeman modulation was derived for the case $I=1$ and $\eta=0$, it should be equally valid for all integral-spin, $\eta=0$, cases. Furthermore, for half-integral spins it should also be applicable if transitions to $m=\pm\frac{1}{2}$ levels are not involved. The applicability of the theory will be further discussed below.

D. Frequency Modulation, Phase-Sensitive Detection, Absorption Signal

We consider frequency modulation (FM) briefly since it is an often-used technique to which the present theory is easily applied. Let us treat separately the cases of no magnetic field and static magnetic field. For FM the frequency parameter β becomes

$$\beta+\beta_m \cos\omega_m t.$$

1. *No Magnetic Field* $(\Omega=0)$

a. Single crystal. Equation (44) becomes for $\theta=0$:

$$M_{x'}=\frac{2C}{1+\Delta\omega^2 T_2^2},$$

which, as we have already seen, is the usual Lorentzian expression. For FM ($\Delta\omega\rightarrow\Delta\omega+f\cos\omega_m t$) the theoretical treatment for line shape and width is exactly that already given for Lorentzian magnetic resonance signals and magnetic modulation.[27–29] The treatment for frequency modulation of Gaussian NQR lines is expected to be just that for magnetic resonance.[27–29] We shall not discuss these cases further except to remark that signal amplitude and linewidth plots as a function of modulation amplitude are given in Ref. 29. In using these plots it is necessary to replace the modulation and linewidth parameters $h_m/\delta H$, $\delta H_{\text{meas}}/\delta H$, and $\delta H_{\text{meas}}/h_m$ of Ref. 29 by the quantities $f/\delta\omega$, $\delta\omega_{\text{meas}}/\delta\omega$, and $\delta\omega_{\text{meas}}/f$.

b. Polycrystal. Averaging Eq. (44) over θ and ψ gives the polycrystal result

$$\bar{M}_{x'}=\frac{4C}{3(1+\Delta\omega^2 T_2^2)},\tag{49}$$

which is just $\frac{2}{3}$ the optimum single crystal value, as expected.[42] Hence, the behavior of both single crystal and polycrystal NQR FM signals as a function of modulation is given in Ref. 29, at least for Lorentzian and Gaussian lines.

2. *Static Magnetic Field* $(\Omega\neq 0)$

a. Single Crystal. In Eq. (43) we again have $\Delta\omega\rightarrow\Delta\omega+f\cos\omega_m t$. Letting $\beta=\Delta\omega T_2$, $\beta_m=fT_2$, $\epsilon_s=\Omega_s T_2=\gamma h_s T_2$, and $s=1$, we get

$$M_{x'}=\frac{2C[1+(\beta+\beta_m\cos\omega_m t)^2+\epsilon_s^2\cos^2\theta](1-\sin^2\psi\sin^2\theta)}{[1+(\beta+\beta_m\cos\omega_m t+\epsilon_s\cos\theta)^2][1+(\beta+\beta_m\cos\omega_m t-\epsilon_s\cos\theta)^2]}.\tag{50}$$

---

[42] Reference 12, p. 328.

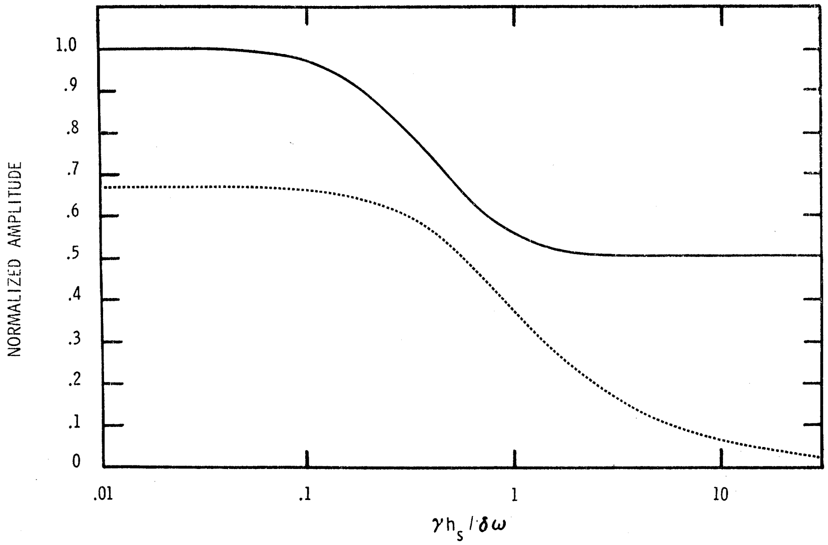

FIG. 18. Effect of static magnetic field on theoretical single crystal and polycrystal derivative signal amplitude for frequency modulated signals. The curve for a single crystal optimally oriented is solid, that for the polycrystal is dashed.

The optimum magnetization, of course, occurs for Z and Z' axes coincident ($\theta=0$). The theoretical observed signal is again a_1 as found by substitution of Eq. (50) into Eq. (28) (replacing $M_{y'}$ by $M_{x'}$). The resulting integral identically vanishes for either $\beta=0$ or $\beta_m=0$, as it should to agree with experiment since the signal is zero at the center frequency and also zero if the modulation amplitude is zero.

The theoretical observed signal for an optimally oriented single crystal, as calculated from Eq. (50), is qualitatively similar to that calculated for nuclear induction in the presence of a static field. In fact, a comparison of the two signal shapes at $\gamma h_s/\delta\omega=1.732$ shows little quantitative difference. However, the difference in angle dependence between Eq. (50) and Eq. (16) results in marked deviations in the behavior with h_s of the polycrystal signals for the two methods.

The theoretical FM signal, as h_s increases, shows splitting which can be regarded as the superposition of two derivative signals. As $h_s\to\infty$, each half-signal tends to half the zero field amplitude. The theoretical behavior of the peak amplitude is shown (for optimum crystal orientation) in Fig. 18 and Table IV. Also given in Table IV are the theoretical parameters for the linewidth measured between extrema.

b. Polycrystal. Averaging Eq. (43) over θ and ψ gives as the polycrystal magnetization:

$$\bar{M}_{x'}=\frac{C}{2}\left\{\frac{2}{\epsilon_s^2}-\frac{\beta}{\epsilon_s^3}\ln\frac{1+(\beta+\epsilon_s)^2}{1+(\beta-\epsilon_s)^2}+\frac{\beta^2+\epsilon_s^2-1}{\epsilon_s^3}[\tan^{-1}(\beta+\epsilon_s)-\tan^{-1}(\beta-\epsilon_s)]\right\}. \quad (51)$$

Letting $\beta\to\beta+\beta_m\cos\omega_m t$, we find in solving for a_1 that the first term integrates to zero. The polycrystal signal for phase-sensitive detection thus becomes

$$a_1=\frac{C}{\pi\epsilon_s^3}\int_0^\pi\left\{(\beta+\beta_m\cos\theta_m)\ln\frac{1+(\beta+\beta_m\cos\theta_m-\epsilon_s)^2}{1+(\beta+\beta_m\cos\theta_m+\epsilon_s)^2}+[(\beta+\beta_m\cos\theta_m)^2+\epsilon_s^2-1][\tan^{-1}(\beta+\beta_m\cos\theta_m+\epsilon_s)-\tan^{-1}(\beta+\beta_m\cos\theta_m-\epsilon_s)]\right\}\cos\theta_m d\theta_m, \quad (52)$$

where $\theta_m=\omega_m t$. As is required of a physically correct solution, Eq. (52) integrates to zero if either $\beta=0$ or $\beta_m=0$. Like the induction and single-crystal FM signal, the polycrystal signal shows complex structure at large static-field amplitudes. The line splits into

TABLE IV. Calculated effect of static magnetic field on linewidth and signal amplitude for experiments using frequency modulation and phase-sensitive detection.

	Single Crystal ($\theta=0$)			Polycrystal		
$\frac{\gamma h_s}{\delta\omega}$	$\frac{\delta\omega_{\text{meas}}}{\delta\omega}$	$\frac{\delta\omega_{\text{meas}}}{\gamma h_s}$	Norm. Amp.	$\frac{\delta\omega_{\text{meas}}}{\delta\omega}$	$\frac{\delta\omega_{\text{meas}}}{\gamma h_s}$	3× (Norm. Amp.)/2
0.02598	1.005	38.7	1.000	1.005	38.7	1.000
0.04330	1.010	23.3	0.996	1.008	23.3	0.999
0.08660	1.031	11.9	0.980	1.013	11.7	0.992
0.1732	1.126	6.50	0.922	1.048	6.05	0.967
0.3464	1.472	4.25	0.774	1.195	3.45	0.880
0.5196	1.905	3.67	0.667	1.420	2.73	0.777
0.6928	2.303	3.33	0.605	1.697	2.45	0.681
0.8660	2.702	3.12	0.570	2.009	2.32	0.600
1.039	3.048	2.93	0.548	2.356	2.27	0.534
1.212	3.395	2.80	0.535	2.667	2.20	0.481
1.386	3.723	2.69	0.525	3.031	2.19	0.440
1.559	4.070	2.61	0.519	3.377	2.17	0.404
2.598	6.235	2.40	0.505	5.37	2.067	0.276
3.464	7.97	2.30	0.503	7.10	2.05	0.220
5.196	11.43	2.20	0.501	10.57	2.03	0.157
6.928	14.90	2.15	0.5007	14.02	2.025	0.123
8.660	18.36	2.12	0.5006	17.32	2.00	0.102
17.32	35.68	2.06	0.5004	34.64	2.00	0.054
34.64	70.32	2.03	0.5004	69.28	2.00	0.029

antisymmetric components, the intensity of which approaches zero as h_s increases. This behavior is, of course, due to the broadening which results from the polycrystal average over angle.

The theoretical behavior of the peak polycrystal derivative amplitude as a function of static magnetic field is shown in Fig. 18 and Table IV. Table IV also gives the theoretical linewidth parameters.

E. Comparison of Theoretical Signal Amplitudes for the Methods

Let us now compare the optimum theoretical signal strengths expected for the various methods, apart from noise considerations. In the absence of a static magnetic field, the maximum theoretical signal strengths for the optimally oriented single crystal and the polycrystal are given in Table V. The experimental conditions are: (1) same H_1 for each method (no saturation), and (2) field or frequency modulation amplitude adjusted for maximum phase-sensitive detected signal. The maximum signal is given in terms of the quantity $C=2\gamma H_1 M_0 T_2$ and does not include the factor ω (as discussed in Sec. II.B.1) or such parameters as gain, filling factor, etc. Actually we are interested in the relative amplitudes of the signals, so that the normalizing constant is of little consequence. Although the polycrystal induction signal is $\frac{1}{3}$ the optimum single crystal value for low modulations, this is not so for the maximum signal because of the angle dependence of the modulation parameter. Since the frequency term contains no angle dependence, the polycrystal FM signal is $\frac{2}{3}$ that of the optimally oriented single crystal for all modulation amplitudes.

Some of the numerical coefficients in Table V may contain small errors due to the approximate nature of the machine integration methods used in their calculation. However, the accuracy is satisfactory for our purposes.

Although the peak single crystal signals for induction and FM are the same, Robinson[2] has shown that the induction method has the better signal-to-noise ratio.

TABLE. V. Theoretical maximum signal strengths for three experimental NQR methods.[a] (No saturation, no static field.)

	Single Crystal ($\theta=0$)		Polycrystal	
Method	Peak signal	Modulation at peak	Peak signal	Modulation at peak
Induction	C	$\frac{\gamma h_m}{\delta\omega}=1.8$	$0.41C$	$\frac{\gamma h_m}{\delta\omega}=1.9$
Zeeman modulation	$\frac{4C}{\pi}=1.27C$	$\frac{\gamma h_z}{\delta\omega}=\infty$	$\frac{8C}{3\pi}=0.85C$	$\frac{\gamma h_z}{\delta\omega}=\infty$
Frequency modulation	C	$\frac{f}{\delta\omega}=1.732$	$\frac{2C}{3}$	$\frac{f}{\delta\omega}=1.732$

[a] Signal is also proportional to frequency ω, as discussed in text.

IX. DISCUSSION, SUMMARY, AND CONCLUSIONS

This section has a twofold purpose; first, to review the applicability of the present theory to the experimental situation for which it was derived; second, to examine the possibility of generalizing the theory to other situations.

A. Applicability of the Method for $I=1$, $\eta=0$

The present theory was derived under several restrictions. These included four major assumptions: (1) nuclear spin $I=1$; (2) electric field gradient cylindrically symmetric about the Z axis ($\eta=0$); (3) relaxation processes parallel to and transverse to the Z axis each describable by single relaxation times; and (4) no spin quenching. The effect of the first two assumptions will be examined below. The third assumption automatically builds into the theory a Lorentzian line shape, and as a result, produces an effect on the agreement between theory and experiment. However, the assumption of single relaxation times is not so restrictive as to prevent the theory from being at least qualitatively (and often quantitatively) correct in all aspects investigated.

1. Induction Experiment (Phase-Sensitive Detection)

The theory gives good quantitative agreement with the experimental results for the dependence of linewidth on both modulation field and static field. The theory is qualitatively correct for the dependence of line shape and signal amplitude on these parameters. The saturation behavior of the signal also shows reasonable agreement between theory and experiment.

Any discrepancies between theory and experiment can reasonably be associated with the non-Lorentzian line shape of the experimental signal or with spin-quenching effects (which are probably minor for hexamethylenetetramine). Unfortunately, it is considerably more difficult to build other line shapes (e.g., Gaussian) into the present theory than into the analogous NMR theory. However, since the main features of the experiment are explained using a Lorentzian line shape, this difficulty is not critical.

A slight modification of the theory indicates that frequency modulation in the presence of a static magnetic field yields an observable signal. For low enough fields the V-mode signal looks like a second derivative of an absorption line.

2. Absorption Experiments

a. Sinusoidal magnetic modulation. Theory predicts that, for sinusoidal magnetic modulation and phase-sensitive detection at the same frequency, the signal is identically zero. An experiment on ^{35}Cl in *p*-dichlorobenzene ($I=\frac{3}{2}$, $\eta=0.08$) confirmed the theoretical result. Since the theory was derived for $I=1$, $\eta=0$, it would be useful to repeat the experiment for ^{14}N in hexamethylenetetramine. However, we expect the theory to be qualitatively applicable to half-integral spins for any η.

b. Zeeman modulation. The present theory gives the proper qualitative line shape for both single crystal and polycrystal samples. The theoretical line shape includes both the positive signal at the resonance center and the negative wings. The work of Negita[13] is more general, including both Lorentzian and Gaussian lines for $\eta\geq 0$, the present work agrees with that of Negita for $\eta=0$ and a Lorentzian line.

c. Frequency modulation. In the absence of static magnetic fields the theory of this method reduces to that for sinusoidal magnetic modulation of Lorentzian magnetic resonance lines as previously considered in Refs. 27–29. The effect of static magnetic fields has been considered in the present work in some detail, and reasonable results for the linewidth, line shape, and signal amplitude obtained.

B. Extension of the Theory to Other Cases

Although the present theory was derived for $I=1$, $\eta=0$, it is possible to extend it qualitatively to other cases without detailed calculations.[43] This can be done by considering the general form of the dependence of resonance frequency upon η and magnetic field for these cases.

1. *Integral Spin Nuclei*

a. $\eta=0$. In the absence of saturation effects the present theory should be as valid for $I=2, 3, 4, \cdots$ as it is for $I=1$. This is true since for these spins also the application of a small magnetic field H produces shifts of the precession frequencies from ω_0 to $\omega_0\pm\gamma H\cos\theta$.

If the rf field H_1 is strong enough to produce saturation, the theory must be altered by changing the squared matrix elements $P^2(=S^2)$ in the saturation parameter[16] $4\gamma^2H_1{}^2T_1T_2P^2\sin^2\theta_1$. The values of P^2 are easily calculable,[22] and so the change in the theory is minor. Das and Hahn[44] discuss relaxation effects in some detail.

b. $\eta>0$. Although the present theory is not applicable to the case $\eta>0$, some general conclusions can be drawn.[43] For η small, the degeneracy of the energy levels is removed linearly with applied magnetic field,[45] as is the case for $\eta=0$. Thus we qualitatively expect, by analogy with the present treatment, that the induction method will work for integral spins, small η, as does the Zeeman-modulated absorption method.[45] However, since the degeneracy is removed quadratically with field for large η, the induction method, like the Zeeman-modulated absorption method[45] fails.

2. *Half-Integral Spin Nuclei*

a. $\eta=0$. Since, for $I=\frac{3}{2}, \frac{5}{2}, \frac{7}{2}, \cdots$, the shift of central precession frequency for all transitions except those to the $m=\pm\frac{1}{2}$ levels is given by Eqs. (15), we expect the present theory to apply in all aspects except saturation. For saturation curves the saturation factor must be adjusted as previously discussed (Sec. IX B 1.a).

If transitions to the $\pm\frac{1}{2}$ levels are involved, the application of a magnetic field mixes the two states so that four transitions (instead of two) between the $\pm\frac{3}{2}$ levels and the new mixed states are now allowed.[21] Although this complicates the picture somewhat, the shift of the new levels is essentially proportional to $\Omega\cos\theta$. Thus, the nuclear induction method should still be applicable, but some structure may be present in the observed signals, due to the involvement of four instead of two levels. One expects this structure to disappear for low enough modulations.

b. $\eta>0$. The degeneracy of quadrupole energy levels for half-integral spins is not removed by nonaxial field gradients, but each level is shifted by an amount dependent upon η. The degeneracy is removed linearly by a magnetic field,[46] so the induction method should work for half-integral spins, any η.

ACKNOWLEDGMENTS

The author wishes to thank B. W. Joseph who performed most of the experiments and constructed auxiliary apparatus. I am also grateful to Dr. R. E. Michel and Dr. J. G. Gay for helping me over some obstacles to the mathematical treatment and physical understanding of the problem. I also wish to thank Professor H. S. Gutowsky, Dean K. A. Brueckner, Professor R. M. Deal, Professor S. Alexander, and Dr. D. E. Woessner for useful discussions. The comments of Dr. W. G. Proctor were extremely valuable. Finally the author expresses his appreciation to Dr. N. L. Muench and D. L. Fry for their continued interest and encouragement in this research.

---

[43] The author is grateful to Dr. W. G. Proctor for valuable comments pertinent to this discussion.

[44] Reference 6, p. 60.

[45] P. A. Casabella and P. J. Bray, J. Chem. Phys. **28**, 1182 (1958); **29**, 1105 (1958).

[46] Reference 6, p. 19.